Reliability Engineering and System Safety 230 (2023) 108878

Contents lists available at ScienceDirect

Reliability Engineering and System Safety

journal homepage: www.elsevier.com/locate/ress

Civil aircraft engine operation life resilient monitoring via usage trajectory mapping on the reliability contour☆

Hang Zhou [a,b,*], Maryam Farsi [c], Andrew Harrison [d], Ajith Kumar Parlikad [b], Alexandra Brintrup [b]

[a] James Watt School of Engineering, University of Glasgow, UK
[b] Institute for Manufacturing, Department of Engineering, University of Cambridge, UK
[c] School of Aerospace, Transport and Manufacturing (SATM), Cranfield University, UK
[d] Rolls-Royce plc, Derby, UK

ARTICLE INFO

Keywords:
Reliability
Aviation operations
Aircraft propulsion system
Fleet management
Optimization

ABSTRACT

The civil aircraft engine business is complex in operation. Being an asset-heavy business operating highly complex engineering systems, the optimized fleet life-cycle management is essential yet challenging. The aviation systems are known for critical operation conditions, high-standard reliability demands, and high cost in both asset value and through-life maintenance services. Civil aircraft engines typically require 3 to 4 highly costly overhauls through service life to maintain performance and the time-on-wing (TOW) requirements of the airline operators. Multiple levels of maintenance activities need accurate and long-term planning for engine fleets coordinating manufacturing, transportation, supply chains and system performance, based on the service life of the engines. The life of assets in the aviation industry is measured uniquely by two scales — the flying hour (FH) and the flying cycle (FC). This paper proposed to evaluate the aviation systems' service life combining both FH and FC, and the reliability of the systems be dynamically quantified via the records and future plans of the flight profiles. The long-term planning of the most significant shop visit (SV) overhauls is therefore optimized by maximizing the fleet TOW availability, considering the business model of 'charge customers by the flying time' in the civil aircraft engine business.

1. Introduction

The reliability and safety of the transportation systems are vital and fundamental for human society and civilization, and among all the reliability evaluation approaches, one of the most important and popular benchmark is the remaining useful life (RUL) of the systems [1]. Therefore, the study of RUL in transportation systems, their sub-systems and core components have attracted wide research interest. Among all transportation forms, air travel is considered as the most efficient way for long distance traveling. The aviation industry is an asset-heavy industry, with high cost in both the asset value and life-cycle operation. In reality, the everyday operation by airlines are complex, with one core factor that governs the airline operation being the condition and health of the aircraft. Out of all the advanced systems integrated in the manufacturing of aircraft, the aircraft propulsion system is considered as the core system. Aircraft propulsion system, or within the commercial aviation industry, often being referred to as the civil aircraft engine, is known for its high complexity in designing & manufacturing, high reliability requirements, extreme operating conditions, high asset value and high operational cost. To ensure the aircraft engines maintain highly reliable and stays at the peak performance, the engines are set to go through multiple levels of maintenance throughout the life-cycle. Among all the levels, the highest level of maintenance is the overhaul, where the engines are refurbished to as-new conditions. Overhaul activities are highly costly, both economically and in duration of time. At the same time, they are highly critical as the accurate planning of overhaul activities lead to the minimum disruptions for airline operators, avoiding high penalty of unplanned events and generate more flying time for engine manufacturers and maintenance service providers. More importantly, well planned overhaul activities allow the aviation industry to operate at top safety level, and the maintaining of peak performance guarantees the designed efficiency, which limits excessive carbon emissions by aviation operations. With the consideration of both high performance and cost-effective life-cycle management of civil aircraft engines, there are two important aspects influencing the decision making: the condition & health status of the asset, which ensures the safety of the aircraft operation; and the RUL of the asset, which determines the

☆ This research is funded by the Aerospace Technology Institute (ATI) and Innovate UK.
* Corresponding author at: James Watt School of Engineering, University of Glasgow, UK.
E-mail address: Hang.Zhou@glasgow.ac.uk (H. Zhou).

https://doi.org/10.1016/j.ress.2022.108878
Received 21 March 2022; Received in revised form 15 July 2022; Accepted 30 September 2022
Available online 26 October 2022

availability of the aircraft fleet. In order to operate smoothly with minimum disturbance, long-term predictability is vital in fleet planning for the aviation industry. Core components, for example, the large diameter fan case and HPT (high pressure turbine) blades can take a year to manufacture and transport to the overhaul facilitates. The responsive speed as well as the awareness of the future availability for a fleet is key for the airline operators to arrange flight schedules, and more importantly, to fulfill the target flying time. The understanding of the combined information of aircraft engine health condition, the remaining operable time before overhaul, availability rate of a fleet, and the anticipated unavailable time window at any given time in the long-term future is the quantified understanding of the RUL of each engine in the fleet, and is the foundation of the resilience analysis of the aircraft engine fleets, which is fundamental to direct the operational decision making.

Currently, one focus of the RUL estimation of the complex transportation systems is typically by the natural time measurement, including years, days, hours, seconds etc. Research on such systems with natural time measurement for service life include the life of electric bus fleet in the measurement of years [2], the aircraft cooling system in days [3], and key components in the systems like bearings [4,5] by the measurement of hours and seconds. Apart from the natural time, another type of life measurement that is common for the transportation system is the count of operational cycles. For example, the usage of railway D-cables [6], and research on popular datasets of C-MAPSS [7–9]. Moreover, with the future next generation transportation systems shifting towards being electrical, the operation time of the lithium-ion batteries are measured with recharging cycles [10,11]. However, in the current aviation operations, the service life of the aircraft engines are uniquely measured by both the natural time measurement and the count of operational cycles, considering the multiple deterioration mechanism and failure modes on the transportation systems. According to the current studies, core components within the aircraft engines under cyclic loading suffer from fatigue-induced crack propagation, which is examined by studies targeting on sub-systems such as crankshaft of helicopter engines [12] as well as the combustor of the aircraft engines [13]. The failure mechanism that is cyclic-loading related leads to the life estimation of such components are measured by the count of operation cycles. Different from the cycle-based failure mechanisms, solid-material components in aircraft engines work and are exposed constantly to high-intensity stress along with extremely high temperatures. Due to the extreme operational conditions, creep is one common failure mechanism being widely studied for aviation systems, and are investigated on components like low-pressure turbine blade failures [14] and turbine disk failures, particularly on the widely used nickel-based superalloy material for such components [15–17]. The life estimation of time duration-related failure mechanisms is majorly measured in hours of usage, which is a natural time duration. There are currently few studies carried out on the combination of the multiple life measurement scales, with Zhou et al. [18] provided the initial concept. This means that a gap exists in the joint evaluation of the transportation system service capabilities by combining the multiple time scale life measurements.

The joint evaluation has the potential to re-shape the existing lifecycle management in the aircraft engine industry, as it provides a new understanding of the asset performance, providing theoretical support on the novel insights in estimating both the consumed life and the remaining useful life of the engines. In the literature, the determination of maintenance timelines and schedules, for both the planned predictive maintenance and condition-based maintenance, are comprehensively studied on railway systems [19,20]. As for the civil aircraft engines, this reliability estimation determines the time-based overhaul interval, by providing the reliability threshold which is associated to both the FC and the FH. In reality, the reliability threshold is difficult to determine, as maintenance strategies based on the reliability threshold is often pre-defined with empirical knowledge instead of calculated. This pre-defined reliability threshold based maintenance schedule is studied on railway network maintenance scheduling with the usage time in months [21], and on the preventive maintenance for machine scheduling problem with consideration of availability [22]. However, different approaches have been investigated towards a variety of engineering systems. An approach to determine the system failure threshold based on the long-run cost rate is proposed and the maintenance policy is calculated on an asphalt plug in a bridge system, for which the service life is one-dimensional and is estimated by the years of usage [23]. Further to this, the maintenance threshold to both maximize the energy-based availability and reduce the life cycle cost, on the operation of wind farms is proposed [24], and on high-voltage underground power transmission cables [25]. It is worth noticing that, the determination of reliability threshold, as the benchmark determination of the end of assets' life, focuses on the one-dimensional service life calculation. With the joint evaluation model, the calculation of the maintenance schedules, regarded as a interim end-of-life benchmark, is at the same time, an existing research gap.

Therefore,responding to the industrial and research challenges, this paper intends to make the following contributions:

(1) A combined contribution of multiple failure mechanism is studied on a fleet of civil aircraft engines based on the real-life service data provided by our industrial partner Rolls-Royce plc., on the most widely used civil aircraft engines among international airline operators. The reliability evaluation of the aircraft engines is studied with a variety of root causes for system removals and overhauls. By introducing the comprehensive reliability estimation on both FC and the FH with multiple failure mechanisms, the reliability evaluation through life-cycle is modeled by copula. This paper proposes a non-parametric estimation of the association measurement parameter for copula modeling based on Monte-Carlo simulation, in order to improve the model accuracy and neutralize over fitting of such models. The copula based reliability model is further developed into a reliability contour map to simplify the condition-based monitoring of the health state of aircraft engine operations.
(2) In order to obtain beneficial the maintenance planning strategies for fleets of civil aircraft engines, it is important to provide long term predictability of maintenance timing and scheduling to avoid the costly penalties upon unplanned failure events. It is also the design purpose of the aircraft engines to fulfill the demanded flying time annually for the effective and efficient operations of airline operators. Based on the reliability contour map, the end-of-service-cycle threshold is defined and calculated, with the target to maximize the availability of the aircraft engine fleet, which in another explanation, is the time between overhaul of the aircraft engines. The threshold calculation in order to maximize the availability with the information of copula reliability model is solved by a proposed iteration algorithm. The obtained end-of-service-cycle threshold is further used for the estimation of RUL for each individual engine during operations.
(3) A visualization tool for civil aircraft engine health monitoring is further developed based on the reliability contour map. This tool combines the information of quantified aircraft engine reliability evaluation, the overhaul interval threshold, and the real-life RUL calculation with both the remaining FH and FC according to the aircraft flying profiles. The tool possess the capability to monitor each individual aircraft engine, as well as the fleet of engines when the resilience of the fleet is vital for the decision making.

The paper is structured as follows: In Section 2 we discuss the methodology in three sub-sections: the reliability contour map development, the overhaul interval determination on maximized system availability, the engine health state monitoring & fleet resilient monitoring. In Section 3 we provide the results and discussion with a case study on one of the most popular civil aircraft engine products by our industrial partner Rolls-Royce plc., based on the real life operational data. In Section 4 we conclude the paper and further provide information of our ongoing work.

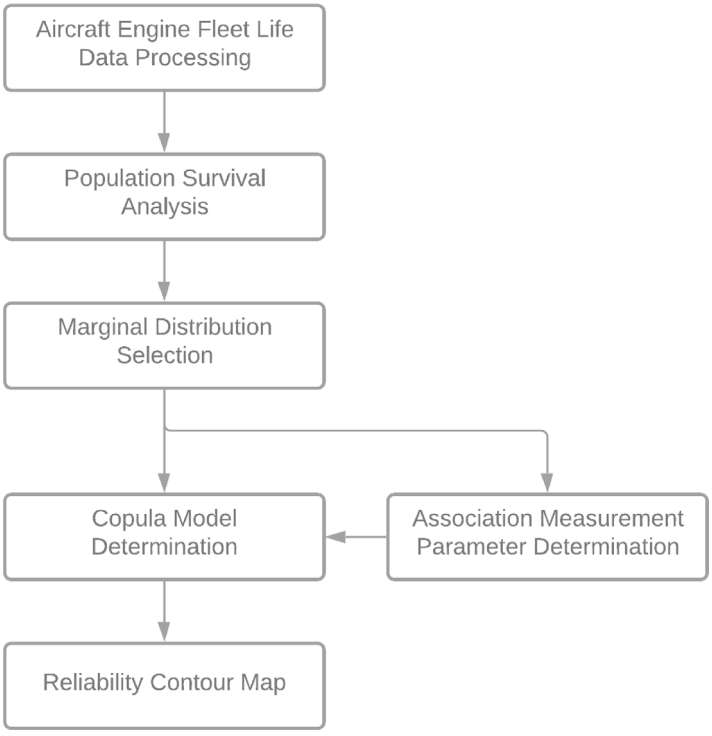

Fig. 1. Steps for the deduction of reliability contour map for aircraft engine usage monitoring.

2. Methodology

In the methodology section, three major steps are described. First we provide the reliability contour map development, for its applicability in real life aircraft engine usage monitoring. Second, we showcased the model and solution algorithms to determine the aircraft engine overhaul interval based on the maximum availability of such systems. And third of all, we mathematical define trajectory of engine usage and demonstrate the mapping of the usage trajectory overlaying the reliability contour map. The application of this real-life monitoring tool on single engine health state and fleet resilience is also defined and demonstrated.

2.1. Reliability contour map

In order to develop a monitoring tool based on the reliability contour map, steps need to be take as shown in Fig. 1.

2.1.1. Aircraft engine fleet life data processing

Assume there is a dataset containing a population of civil aircraft engine maintenance records, each record is associated with the FH and the FC upon an overhaul is carried out due to failure detection. All the engines in the dataset is of the same design, or in another word, is of the same engine design model. The dataset is in the format of: engine i has service time record $(t_{h_i}, t_{c_i}), i = 1, 2, \ldots, n$, where t_{h_i} (hour) and t_{c_i} (cycle) are engines' safe service life before failure, measured by both the FH and FC, and n is the population of engines of the same design in the maintenance record.

Both of the FH and FC measurements in the dataset are rational numbers. In order to enable both measurements have the same weighted contribution towards the estimation of the engines' life, the data is first normalized. The FH with set $\mathbf{T_h} = (t_{h_1}, t_{h_2}, \ldots, t_{h_n})$ and FC with set $\mathbf{T_c} = (t_{c_1}, t_{c_2}, \ldots, t_{c_n})$, the maximum engine capability in both time scales are the largest samples within each set with $t_{h_{max}} = max\{t_{h_1}, t_{h_2}, \ldots, t_{h_n}\}$ and $t_{c_{max}} = max\{t_{c_1}, t_{c_2}, \ldots, t_{c_n}\}$. The minimum values for both time scales are 0. Both sets after normalization are:

$$\begin{cases} \mathbf{T_{c_{norm}}} = \left(\frac{t_{c_1}}{t_{c_{max}}}, \frac{t_{c_2}}{t_{c_{max}}}, \ldots, \frac{t_{c_n}}{t_{c_{max}}} \right) \\ \mathbf{T_{h_{norm}}} = \left(\frac{t_{h_1}}{t_{h_{max}}}, \frac{t_{h_2}}{t_{h_{max}}}, \ldots, \frac{t_{h_n}}{t_{h_{max}}} \right) \end{cases} \tag{1}$$

2.1.2. Population survival analysis

With the FH and FC leveled at the same contribution to an aircraft engine's service capability, the capability can be quantified as:

$$C_i = \|\overrightarrow{C_i}\| = \sqrt{\left(\frac{t_{c_i}}{t_{c_{max}}} \right)^2 + \left(\frac{t_{h_i}}{t_{h_{max}}} \right)^2} \tag{2}$$

where $\overline{C_i} = (\mathbf{T}_{\mathbf{c}_{\mathbf{norm}_i}}, \mathbf{T}_{\mathbf{h}_{\mathbf{norm}_i}}), i = 1, 2, \ldots, n$. Combine C_i values with the associated t_{ci} and t_{hi} to create set $\mathbf{C} = (\mathbf{T}_{\mathbf{c}_{\mathbf{norm}}}, \mathbf{T}_{\mathbf{h}_{\mathbf{norm}}}, \mathbf{c})$. Rearrange $\mathbf{C}$ according to the values of C_i in $\mathbf{c}$ as a monotonic increasing set of values, we have $\mathbf{C}' = (C_1, ..., C_j, \ldots, C_n)$, $\mathbf{C}' = \mathbf{C}$ and $C_j \leq C_{j+1}$, the two normalized time scale measurement associated with capability C_j are $(\mathbf{T}_{\mathbf{c}_{\mathbf{norm}_j}}, \mathbf{T}_{\mathbf{h}_{\mathbf{norm}_j}})$. A survival analysis [26] is performed on the dataset with the consideration of the capability calculation in Eq. (2) as:

$$\mathbf{R}(C_j) = \hat{S}(C_j) = \prod_{j:C_j \leq C_{max}} \left(1 - \frac{d_j}{n_j}\right) \tag{3}$$

Here d_j is the number of products recorded as failure at C_j, n_j is remaining number of products in the population. The output of Eq. (3) $\mathbf{R}(C_j)$ is the reliability of the product at C_j, creating a three dimensional description of each recorded datapoint with $\mathbf{S} = (\mathbf{x}, \mathbf{y}, \mathbf{z}) = (\mathbf{T}_{\mathbf{c}_{\mathbf{norm}_j}}, \mathbf{T}_{\mathbf{h}_{\mathbf{norm}_j}}, \mathbf{R}(C_j))$, on the x-axis, y-axis and z-axis of a Cartesian coordinate system.

2.1.3. Marginal distribution selection

In order to construct a model integrating both the contributions of the FH and FC, copula is an effective approach. The copula model, according to the Sklar's Theorem [27], let F be a bivariate joint distribution function of continuous random variable X and Y with corresponding marginal distribution functions F_1 and F_2. There exists a copula $\mathscr{C}$ such that, for $-\infty < x_1 < \infty, -\infty < x_2 < \infty$, there is $F(x_1, x_2) = P(X_1 \leq x_1, X_2 \leq x_2) = \mathscr{C}(F_1(x_1), F_2(x_2))$. The choice of marginal distributions for both time scales is in need. In the research of reliability and risk assessment, four formats of distributions are proved to be the most widely used. They are the GEV distribution, the Weibull distribution, the Gumbel distribution and the Normal distribution. The general formats of these four distributions are given as the target reliability functions.

Target reliability function of GEV distribution:

$$R(t) = 1 - e^{-\left[1+\xi\left(\frac{t-\mu}{\sigma}\right)\right]^{-1/\xi}} \tag{4}$$

Target reliability function of Weibull distribution:

$$R(t) = e^{-(t/\sigma)^{\xi}} \tag{5}$$

The target reliability function of Gumbel distribution:

$$R(t) = 1 - e^{-e^{-(t-\mu)/\sigma}} \tag{6}$$

The target reliability function of Normal distribution:

$$R(t) = 1 - \frac{1}{2}\left[1 + \frac{2}{\sqrt{\pi}} \int_0^{\frac{t-\mu}{\sigma\sqrt{2}}} e^{-l^2} dl\right] \tag{7}$$

For all the distribution formats given in Eqs. (4)–(7), μ is the location parameter, σ is the scale parameter and ξ is the shape parameter. The choice of marginal distribution relies on the format that achieves the minimum coefficient of determination $\mathscr{R}^2$ value regarding all the datapoints in $\mathbf{S}$.

2.1.4. Copula model determination & association measurement parameter determination

From step (2.1.3), consider F_1 and F_2 are the marginal distributions describing the reliability of the product with time usage on each time scale, with F_1 describing the FH axis and F_2 describing the FC axis. ϕ is the association measurement parameter related to the format of the copula model. The common format of copula models is briefly introduced here, all belong to the Archimedean copula family.

2.1.4.1 Gumbel copula: For a bivariate distribution, the Gumbel copula [28] is expressed as:

$$F(t_c, t_h) = exp\left\{-\left[\left(-logF_1(t_c)\right)^{\phi} + \left(-logF_2(t_h)\right)^{\phi}\right]^{1/\phi}\right\} \tag{8}$$

The Gumbel copula demonstrates a type of copula with just one corner of the tail dependence. It is also worth noticing that one key characteristics of bivariate copula models is the calculation of the association measurement parameter ϕ, which describes the association relationship between the bivariate variables. For the Gumbel copula, $\phi \in [1, \infty)$.

2.1.4.2 Clayton copula: The bivariate Clayton copula [29] is with the format of:

$$F(t_c, t_h) = \left[F_1(t_c)^{-\phi} + F_2(t_h)^{-\phi} - 1\right]^{-1/\phi} \tag{9}$$

For the Clayton copula, $\phi \in [-1, \infty)$ & $\phi \neq 0$.

2.1.4.3 Independence copula: When the association measurement parameter in the Gumbel copula $\phi = 1$, or when the parameter in the Clayton copula $\phi \to 0$. A special type of copula is created which is the independent copula. With the format of:

$$F(t_c, t_h) = F_1(t_c)F_2(t_h) \tag{10}$$

It is obvious that the independence copula is free from the control of ϕ.

Table 1
Relationship between association measurement parameter ϕ and Kendall's τ for four copula models.

Copula model	Kendall's τ
Gumbel	$\tau = \frac{\phi-1}{\phi}$
Clayton	$\tau = \frac{\phi}{\phi+2}$
Independence	NaN
Frank	$\tau = 1 - \frac{4}{\phi}\left(1 - \frac{1}{\phi}\int_0^{\phi} \frac{t}{e^t-1}dt\right)$

Table 2
Association measurement parameter ϕ calculation for four copula models.

Copula model	Association measurement parameter ϕ
Gumbel	$\phi = \frac{1}{1-\tau}$
Clayton	$\phi = \frac{2\tau}{1-\tau}$
Independence	NaN
Frank	Numerical solution

Table 3
Function map of variate for reliability contour determination on fixed value r.

Copula model	$t_h \leftarrow \mathscr{G}(t_c) \leftarrow {F_2}^{-1}(t_c)$
Gumbel	$t_h = {F_2}^{-1}\left(exp\left(-\left((-logr)^{\phi} - (-log{F_1}(t_c))^{\phi}\right)^{1/\phi}\right)\right)$
Clayton	$t_h = {F_2}^{-1}\left(\left(r^{-\phi} - ({F_1}(t_c))^{-\phi} - 1\right)^{-1/\phi}\right)$
Independence	$t_h = {F_2}^{-1}\left(r({F_1}(t_c))^{-1}\right)$
Frank	$t_h = {F_2}^{-1}\left(-\frac{1}{\phi}log\left(1 + \frac{(e^{r\phi}-1)(e^{-\phi}-1)}{e^{-\phi{F_1}(t_c)}-1}\right)\right)$

2.1.4.4 Frank copula: The fourth copula model being considered in this paper is the Frank copula, with the expression of:

$$F(t_c, t_h) = \frac{1}{\phi} log\left[1 + \frac{\left(e^{-\phi F_1(t_c)} - 1\right)\left(e^{-\phi F_2(t_h)} - 1\right)}{e^{-\phi} - 1}\right] \tag{11}$$

For the Frank copula, $\phi \in [-1, 1]$ & $\phi \neq 0$.

From the four potential copula model general expressions, it is obvious that in order to obtain an accurate copula model to describe the dataset, the estimation of the association measurement parameter ϕ is key. There are two common approaches of estimating the parameter ϕ, the parametric approach when the two variate have direct and clear relationships, and the non-parametric approach, when the two variate are complicated and have no simple connections. The parametric approach to calculate ϕ is given in Tables 1 and 2.

In both Tables 1 and 2, one fundamental calculation regarding the two variate is the rank calculation using the Kendall's τ approach, defined as $\tau = \frac{n_c - n_d}{\sqrt{(n_0 - n_1)(n_0 - n_2)}}$, where $n_0 = \frac{n(n-1)}{2}$, $n_1 = \sum_i \frac{t_i(t_i-1)}{2}$, $n_2 = \sum_j \frac{u_j(u_j-1)}{2}$, n_c is the number of concordant pairs, n_d is the number of discordant pairs, t_i is the number of tied values in the ith group of ties for the first quantity, and u_j is the number of tied values in the jth group of ties for the second quantity. The parametric approach in this paper is regarded as a benchmark calculation.

As introduced, the contribution and relationship between the FH and FC towards the aircraft engine performance and capability evaluation are not clearly quantified, meaning the parametric copula model may not perform well statistically to describe the relationship between the two time variate. To address this difficulty, we propose the non-parametric approach to estimate the association measurement parameter in copula models with Monte Carlo simulation, as described in Algorithm 1.

2.1.5. Reliability contour map

Step (2.1.1)–(2.1.4) determines the optimized choice of copula format F, the optimized association measurement parameter ϕ_{opt}, the optimized marginal distribution for time scale 1, noted as F_1, the optimized marginal distribution for time scale 2, noted as F_2. The reliability surface model for the aircraft engine model is:

$$R(t_c, t_h) = F(F_1(t_c), F_2(t_h) : \phi_{opt}) \tag{12}$$

The reliability surface is a model of three-dimensional representation, in order to enable the applicability of such model on engine usage monitoring as well as the fleet resilient monitoring, it is a better approach to perform the dimensional reduction for the three-dimensional reliability surface model to transform into a two-dimensional Cartesian coordinate system, which in this paper we name as the 'reliability contour'. The transformation from a three-dimensional reliability surface to a two-dimensional contour requires the establishment of the relationship between two variables t_c for FC and t_h for FH, with all fixed reliability value r in the domain of $r \in [0, 1]$. Assume $r = F(F_1(t_h), F_2(t_c) : \phi_{opt})$, the relationship between the variables t_h and t_c for all the candidate copula models given from Eqs. (8)–(11) are provided in Table 3.

The determination relationships rely on the inverse function of F_1, which depends on the format of it as a marginal distribution. The inverse functions of all the four candidate marginal distributions are further given.

Inverse function for the GEV distribution is:

$${F_{GEV}}^{-1}(x) = \mu + \frac{\sigma}{\xi}\left((-log(1-x))^{-\xi} - 1\right) \tag{13}$$

Inverse function for the Weibull distribution is:

$${F_{Weibull}}^{-1}(x) = \sigma(-log\ x)^{1/\xi} \tag{14}$$

Algorithm 1 Monte Carlo non-parametric ϕ estimation for copula

procedure ESTIMATION
  for $i \leftarrow 1, v$ **do**
    $\mathbf{D} \leftarrow (\mathbf{T_{1norm}}, \mathbf{T_{2norm}}, \mathbf{C})$ ▷ the processed dataset follows equation (4)
    $\mathbf{N} \leftarrow [1, 2, ..., n]$ ▷ Set of dataset labels with size n
    $\mathbf{N_{tr}} \leftarrow \text{roundup}(p \times n)$ Integer(Random(1, n)) ▷ p is a percentage separating training set data label
    $\mathbf{N_{val}} \leftarrow \mathbf{N_{tr}}^{C}$ ▷ consider set **N** is Universe and set $\mathbf{N_{val}}$ is the Complement of set $\mathbf{N_{tr}}$
    $\mathbf{D_{tr}} \leftarrow \mathbf{D}[\mathbf{N_{tr}}]$ ▷ training dataset
    $\mathbf{D_{val}} \leftarrow \mathbf{D}[\mathbf{N_{val}}]$ ▷ validation dataset
    $\phi_1 \leftarrow \phi_{initial} \leftarrow \phi_{Parametric}$ ▷ set initial search value of ϕ
    for $l \leftarrow 2, \infty$ **do**
      for $u \leftarrow 0, 4$ **do**
        $\phi_l \leftarrow \phi_{l-1} + \frac{1}{10^u}$
        $R[l] \leftarrow \left\{ 1 - \frac{\sum_{i_{tr}} \left\{ \mathbf{D_{tr}}[i_{tr},3] - F(F_1,F_2)|_{x=\mathbf{D_{tr}}[i_{tr},1],y=\mathbf{D_{tr}}[i_{tr},2]} \right\}^2}{\sum_{i_{tr}} \left\{ \mathbf{D_{tr}}[i_{tr},3] - \frac{\sum_{i_{tr}} \mathbf{D_{tr}}[i_{tr},3]}{roundup(p \times n)} \right\}^2} \right\}\Bigg|_{\phi_l}$
        $l \leftarrow l + 1$
        $d \leftarrow R[l] - R[l-1]$
        $r \leftarrow \frac{R[l]-R[l-1]}{R[l-1]}$
        if $d \le 0$ **then**
          $u = u + 1$
        else if $r \le \rho$ **then** ▷ ρ is increment threshold
          BREAK
        end if
      end for
    end for
    $\phi_{Optimize} \leftarrow \phi_l$
    $\mathbf{\Phi}[i] \leftarrow \phi$
    ${R_{val}}^2 \leftarrow \left\{ 1 - \frac{\sum_{i_{val}} \left\{ \mathbf{D_{val}}[i_{val},3] - F(M_1,M_2)|_{x=\mathbf{D_{val}}[i_{val},1],y=\mathbf{D_{val}}[i_{val},2]} \right\}^2}{\sum_{i_{val}} \left\{ \mathbf{D_{val}}[i_{val},3] - \frac{\sum_{i_{val}} \mathbf{D_{val}}[i_{val},3]}{n - roundup(p \times n)} \right\}^2} \right\}\Bigg|_{\phi}$ ▷ obtain R^2 for validation dataset by ϕ
    $\mathbf{R_{val}}[i] \leftarrow {R_{val}}^2$
  end for
  $\mathbf{U} \leftarrow [\mathbf{\Phi}, \mathbf{R_{val}}]$
  $\mathbf{U} \leftarrow$ sort $\mathbf{R_{val}}$ ▷ rank elements in **U** by R_{val} small to large
  $\mathbf{U}' \leftarrow \mathbf{U}[v - q, v]$ ▷ top q performance copula model
  $\phi \leftarrow \frac{\sum_{j=1}^{q} \mathbf{U}'[1,j]}{q}$
end procedure

Inverse function for the Gumbel distribution is:

$$ {F_{Gumbel}}^{-1}(x) = \mu - \sigma log(-log(1-x)) \tag{15} $$

The format of the risk distribution in the format of normal distribution does not have a direct analytical inverse function, however, it can be approximated by Proposition 1.

Proposition 1. *A reliability model in the format of normal distribution has a inverse function and can be approximated by a combination of elementary functions.*

The proof of Proposition 1 is provided in Appendix E.

2.2. Overhaul interval determination

We define the capability of an aviation system as:

$$ W = \frac{L_a}{L_a + L_u} \tag{16} $$

where W is the product capability. L_a is the available life of the system in one overhaul interval and $\|L_a\| = \sqrt{{L_{ac}}^2 + {L_{ah}}^2}$, here L_{ac} is the available life on time scale 1, the FC on t_c-axis, L_{ah} is the available life on time scale 2, the FH on t_h-axis. L_u is the unavailable life of product due to a combined overhaul time consumption and $\|L_u\| = \sqrt{{L_{uc}}^2 + {L_{uh}}^2}$, here L_{uc} is the unavailable life on time scale 1, L_{uh} is the unavailable life on time scale 2. We first focus on the deduction of the available life function.

2.2.1. Product available life

The available lives on both time scales are expressed as:

$$\begin{cases} L_{ac} = E[T_{ac}{}^{*}] + E[T_{ac}{}^{**}] = R(T_c, T_h) \times T_c + [1 - R(T_c, T_h)] \frac{\int_0^{T_c} t_c f(t_c) dt_c}{1 - R(T_c, T_h)} \\ L_{ah} = E[T_{ah}{}^{*}] + E[T_{ah}{}^{**}] = R(T_c, T_h) \times T_h + [1 - R(T_c, T_h)] \frac{\int_0^{T_h} t_h f(t_h) dt_h}{1 - R(T_c, T_h)} \end{cases} \tag{17}$$

In Eq. (17), $E[T_{ac}{}^{*}]$ and $E[T_{ah}{}^{*}]$ represent the expectation of product safe service time without any failure within one overhaul interval for each time scale measurement. $E[T_{ac}{}^{**}]$ and $E[T_{ah}{}^{**}]$ represent the expectation of product safe service time before any failure occurs within one overhaul interval for each time scale measurement. T_c and T_h are the optimum time of overhaul intervals to be determined on both time axis. The value of T_c and T_h determines the product capability W for a new measurement standard of time interval between maintenance. $f(t_c)$ and $f(t_h)$ are the failure probability density functions on both time scales. An assumption is made for the calculation of the available like of engineering product, as seen in Proposition 2. The proof is provided in Appendix F.

Proposition 2. *The available life of engineering product in a bivariate life measurement system L_a is the square root of the squared sum of the two integration of the partial reliability functions $R(t_c, T_h)$ and $R(T_c, t_h)$ deduced from the reliability surface $R(t_c, t_h)$ according to the assumed optimum maintenance time interval on both time scales. Expressed as*

$$L_a = \sqrt{L_{ac}{}^2 + L_{ah}{}^2} = \sqrt{\left[\int_0^{T_c} R(t_c, T_h) dt_c\right]^2 + \left[\int_0^{T_h} R(T_c, t_h) dt_h\right]^2} \tag{18}$$

The proof of Proposition 2 is provided in Appendix F.

2.2.2. Product unavailable life

The product unavailable life is further categorized as the expected unavailable life in both time measurements due to the planned maintenance $E[T_{uc}{}^{*}]\&E[T_{uh}{}^{*}]$, and the expected unavailable life due to the corrective maintenance $E[T_{uc}{}^{**}]\&E[T_{uh}{}^{**}]$ within one overhaul interval. The anticipated unavailable life on both time scales are expressed as:

$$\begin{cases} L_{uc} = E[T_{uc}{}^{*}] + E[T_{uc}{}^{**}] = R(T_c, T_h) \times \bar{M}_{pc} + [1 - R(T_c, T_h)] \times \bar{M}_{cc} \\ L_{uh} = E[T_{uh}{}^{*}] + E[T_{uh}{}^{**}] = R(T_c, T_h) \times \bar{M}_{ph} + [1 - R(T_c, T_h)] \times \bar{M}_{ch} \end{cases} \tag{19}$$

In Eq. (19), $\bar{M}_{pc}$ and $\bar{M}_{ph}$ represent the average life loss due to planned maintenance activities, $\bar{M}_{cc}$ and $\bar{M}_{ch}$ represent the average life loss due to unplanned or corrective maintenance activities. It is generally assumed across multiple industry disciplines that the life loss due to planned maintenance is much shorter than the life loss due to corrective maintenance, which leads to $\bar{M}_{pc} \ll \bar{M}_{cc}$ and $\bar{M}_{ph} \ll \bar{M}_{ch}$.

Therefore, the expected unavailable life within one maintenance interval is:

$$L_u = \sqrt{\left\{R(T_c, T_h) \times \bar{M}_{pc} + [1 - R(T_c, T_h)] \times \bar{M}_{cc}\right\}^2 + \left\{R(T_c, T_h) \times \bar{M}_{ph} + [1 - R(T_c, T_h)] \times \bar{M}_{ch}\right\}^2} \tag{20}$$

The availability model of the aviation systems based on bivariate reliability surface model $R(t_c, t_h)$ is thus deduced as:

$$W = \frac{\sqrt{\left[\int_0^{T_c} R(t_c, T_h) dt_c\right]^2 + \left[\int_0^{T_h} R(T_c, t_h) dt_h\right]^2}}{\sqrt{\left[\int_0^{T_c} R(t_c, T_h) dt_c\right]^2 + \left[\int_0^{T_h} R(T_c, t_h) dt_h\right]^2} + \sqrt{\begin{matrix}\{R(T_c,T_h)\times\bar{M}_{pc}+[1-R(T_c,T_h)]\times\bar{M}_{cc}\}^2 + \\ \{R(T_c,T_h)\times\bar{M}_{ph}+[1-R(T_c,T_h)]\times\bar{M}_{ch}\}^2\end{matrix}}} \tag{21}$$

2.2.3. Solution of model

A necessity condition for availability function W to be optimized to global optimum values, is that the partial differentiation value of both T_c and T_h are 0. In order to approach the global extrema, we propose a heuristic iteration algorithm in this paper towards the solution of the optimization. This algorithm includes a heuristic initial value assignment, and a iterative dynamic grid search, which requires a local extrema obtained at each iteration. It is essential to prove that this algorithm has the ability to obtain the global extrema by Proposition 3, Lemma 1, Corollaries 1.1 and 1.2:

Proposition 3. *The availability function W has global extrema. The optimum value of W can be obtained by a heuristic iteration grid search algorithm.*

Lemma 1. *With any fixed value $T_h{}' \in [0, 1]$, the projection of availability function W on cut-section plane at $T_h{}'$ parallel to plane $t_c - W$ is $W(t_c, T_h{}')$. Function $W(t_c, T_h{}')$ is differentiable and has local extrema.*

Corollary 1.1. *With any fixed value $T_c{}' \in [0, 1]$, the projection of availability function W on cut-section plane at $T_c{}'$ parallel to plane $t_h - W$ is $W(T_c{}', t_h)$. Function $W(T_c{}', t_h)$ is differentiable and has local extrema.*

Corollary 1.2. *Regardless of the heuristic initial assignment value, $(T_c{}^{(0)}, T_h{}^{(0)})$, the local extrema values of each iteration, $(T_c{}^{(n)}, T_h{}^{(n)})$, monotonically increases with the increase of iteration number n.*

The proof of Lemma 1, Corollaries 1.1 and 1.2 and Proposition 3 is provided in Appendix G.

As proved, With each iteration corresponding to the variable of t_c and t_h, the local extrema value is obtained when the partial differentiation is equal to 0:

$$\begin{cases} \frac{\partial W}{\partial T_c} = \frac{\partial W}{\partial L_a}\frac{\partial L_a}{\partial T_c} + \frac{\partial W}{\partial L_u}\frac{\partial L_u}{\partial T_c} = \frac{L_u}{(L_a+L_u)^2}\frac{\partial L_a}{\partial T_c} - \frac{L_a}{(L_a+L_u)^2}\frac{\partial L_u}{\partial T_c} = 0 \\ \frac{\partial W}{\partial T_h} = \frac{\partial W}{\partial L_a}\frac{\partial L_a}{\partial T_h} + \frac{\partial W}{\partial L_u}\frac{\partial L_u}{\partial T_h} = \frac{L_u}{(L_a+L_u)^2}\frac{\partial L_a}{\partial T_h} - \frac{L_a}{(L_a+L_u)^2}\frac{\partial L_u}{\partial T_h} = 0 \end{cases} \tag{22}$$

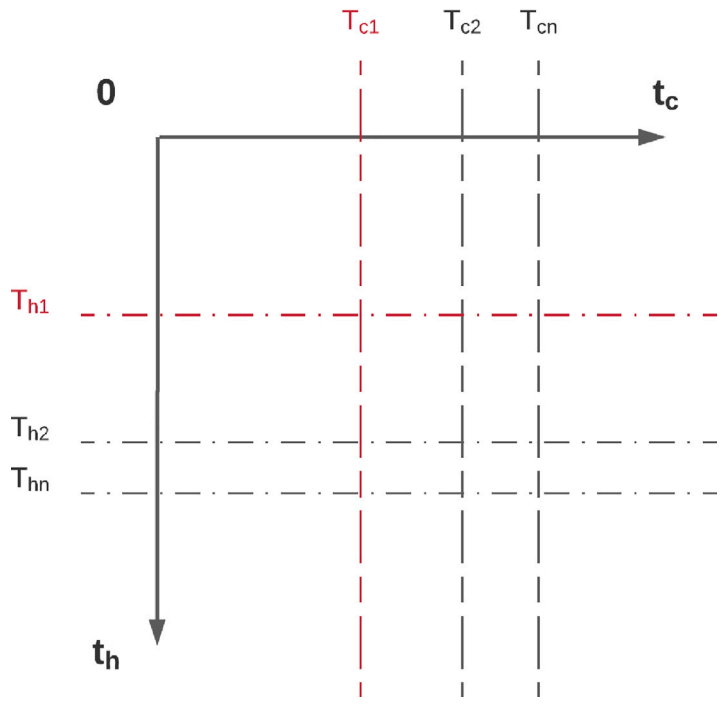

Fig. 2. Iteration algorithm explanation.

which leads to

$$L_u \frac{\partial L_a}{\partial T_c} - L_a \frac{\partial L_u}{\partial T_c} = 0 \tag{23}$$

and

$$L_u \frac{\partial L_a}{\partial T_h} - L_a \frac{\partial L_u}{\partial T_h} = 0 \tag{24}$$

Further deducing Eq. (23), we can obtain:

$$\begin{aligned}
&\sqrt{\left\{R(T_c,T_h)\times \bar{M}_{pc} + [1-R(T_c,T_h)]\times \bar{M}_{cc}\right\}^2 + \left\{R(T_c,T_h)\times \bar{M}_{ph} + [1-R(T_c,T_h)]\times \bar{M}_{ch}\right\}^2}\, \frac{\frac{\partial \int_0^{T_c} R(t_c,T_h)dt_c}{\partial T_c} + \frac{\int_0^{T_h} R(T_c,t_h)dt_h}{\partial T_c}}{(\int_0^{T_c} R(t_c,T_h)dt_c)^2 + (\int_0^{T_h} R(T_c,t_h)dt_h)^2} \\
&- \sqrt{\left[\int_0^{T_c} R(t_c,T_h)dt_c\right]^2 + \left[\int_0^{T_h} R(T_c,t_h)dt_h\right]^2}\, \frac{\left(\bar{M}_{pc} + \bar{M}_{ph} - \bar{M}_{cc} - \bar{M}_{ch}\right)\frac{\partial R(T_c,T_h)}{\partial T_h}}{\sqrt{\left\{R(T_c,T_h)\times \bar{M}_{pc} + [1-R(T_c,T_h)]\times \bar{M}_{cc}\right\}^2 + \left\{R(T_c,T_h)\times \bar{M}_{ph} + [1-R(T_c,T_h)]\times \bar{M}_{ch}\right\}^2}} \\
&= 0
\end{aligned} \tag{25}$$

which gives:

$$\frac{(\int_0^{T_c} R(t_c,T_h)dt_c)^2 + (\int_0^{T_h} R(T_c,t_h)dt_h)^2}{\left\{R(T_c,T_h)\times(\bar{M}_{pc}+\bar{M}_{cc}) + \bar{M}_{cc}\right\}^2 + \left\{R(T_c,T_h)\times(\bar{M}_{ph}+\bar{M}_{ch}) + \bar{M}_{ch}\right\}^2} \frac{\frac{\partial \int_0^{T_c} R(t_c,T_h)dt_c}{\partial T_c} + \frac{\partial \int_0^{T_h} R(T_c,t_h)dt_h}{\partial T_c}}{\left(\bar{M}_{pc}+\bar{M}_{ph}-\bar{M}_{cc}-\bar{M}_{ch}\right)\frac{\partial R(T_c,T_h)}{\partial T_c}} = 1 \tag{26}$$

Apply the same procedure to Eq. (24), we get:

$$\frac{(\int_0^{T_c} R(t_c,T_h)dt_c)^2 + (\int_0^{T_h} R(T_c,t_h)dt_h)^2}{\left\{R(T_c,T_h)\times(\bar{M}_{pc}+\bar{M}_{cc}) + \bar{M}_{cc}\right\}^2 + \left\{R(T_c,T_h)\times(\bar{M}_{ph}+\bar{M}_{ch}) + \bar{M}_{ch}\right\}^2} \frac{\frac{\partial \int_0^{T_c} R(t_c,T_h)dt_c}{\partial T_h} + \frac{\partial \int_0^{T_h} R(T_c,t_h)dt_h}{\partial T_h}}{\left(\bar{M}_{pc}+\bar{M}_{ph}-\bar{M}_{cc}-\bar{M}_{ch}\right)\frac{\partial R(T_c,T_h)}{\partial T_h}} = 1 \tag{27}$$

In order to solve the complex set of partial differential equations (26) and (27), we propose an iteration algorithm as shown in Algorithm 2. There are a few pre-processing key calculations for Algorithm 2 shown below.

2.2.3.1 Key calculations of algorithm: To assist the explanation of this sub-section, Fig. 2 is provided. Assume an established reliability surface model from Eq. (12), given any value T_h within the domain on the t_h axis, a vertical plane at $t_h = T_h$, perpendicular to the $t_h - t_c$ plane and parallel to the t_c axis, intercepts with the reliability surface. The interception produces a projection of distribution curve on the vertical plane with the independent variable of t_c on the t_c axis and the dependent variable of reliability $R(t_c)$. Given any fixed value of T_h, the projected reliability distribution is $R(t_c, T_h)$. The determination of the optimum value of T_c by maximum availability is thus simplified as:

Table 4
Function $\mathscr{F}_{\mathscr{H}}(T_c, t_h)$ and $\mathscr{F}_{\mathscr{C}}(t_c, T_h)$ for four copula model candidates.

Copula Model: Gumbel	
$\mathscr{F}_{\mathscr{C}}(t_c, T_h)$	$-\left\{exp\left\{-[(-logF_1(t_c))^{\phi}+(-logF_2(T_h))^{\phi}]^{1/\phi}\right\}\right\}[(-logF_1(t_c))^{\phi}+(-logF_2(T_h))^{\phi}]^{1/\phi-1}\frac{(-logF_1(t_c))^{\phi-1}}{F_1(t_c)}\frac{dF_1(t_c)}{dt_c}$
$\mathscr{F}_{\mathscr{H}}(T_c, t_h)$	$-\left\{exp\left\{-[(-logF_1(T_c))^{\phi}+(-logF_2(t_h))^{\phi}]^{1/\phi}\right\}\right\}[(-logF_1(T_c))^{\phi}+(-logF_2(t_h))^{\phi}]^{1/\phi-1}\frac{(-logF_2(t_h))^{\phi-1}}{F_2(t_h)}\frac{dF_2(t_h)}{dt_h}$
Copula Model: Clayton	
$\mathscr{F}_{\mathscr{C}}(t_c, T_h)$	$\left[(F_1(t_c))^{-\phi}+(F_2(T_h))^{-\phi}-1\right]^{-(1+\phi)/\phi}F_1(t_c)^{-\phi-1}\frac{dF_1(t_c)}{dt_c}$
$\mathscr{F}_{\mathscr{H}}(T_c, t_h)$	$\left[(F_1(T_c))^{-\phi}+(F_2(t_h))^{-\phi}-1\right]^{-(1+\phi)/\phi}F_2(t_h)^{-\phi-1}\frac{dF_2(t_h)}{dt_h}$
Copula Model: Independence	
$\mathscr{F}_{\mathscr{C}}(t_c, T_h)$	$F_2(T_h)\frac{dF_1(t_c)}{dt_c}$
$\mathscr{F}_{\mathscr{H}}(T_c, t_h)$	$F_1(T_c)\frac{dF_2(t_h)}{dt_h}$
Copula Model: Frank	
$\mathscr{F}_{\mathscr{C}}(t_c, T_h)$	$-\left[e^{-\phi}-1+\left(e^{-\phi F_1(t_c)}-1\right)\left(e^{-\phi F_2(T_h)}-1\right)\right]^{-1}\left(e^{-\phi F_2(T_h)}-1\right)\left(e^{-\phi F_1(t_c)}\right)\frac{dF_1(t_c)}{dt_c}$
$\mathscr{F}_{\mathscr{H}}(T_c, t_h)$	$-\left[e^{-\phi}-1+\left(e^{-\phi F_1(T_c)}-1\right)\left(e^{-\phi F_2(t_h)}-1\right)\right]^{-1}\left(e^{-\phi F_1(T_c)}-1\right)\left(e^{-\phi F_2(t_h)}\right)\frac{dF_2(t_h)}{dt_h}$

$$A_c = \frac{\int_0^{T_c} R(t_c, T_h)dt_c}{\int_0^{T_c} R(t_c, T_h)dt_c + R(T_c, T_h)\bar{M}_{pc} + [1-(R(T_c, T_h))]\bar{M}_{cc}} \tag{28}$$

In order to obtain the most optimum value of T_c, the partial differentiation of A_c is 0 and the Eq. (28) is further deduced as:

$$\frac{\partial A_c}{\partial T_c} = \frac{\partial(\frac{u(t_c,T_h)}{v(t_c,T_h)})}{\partial T_c} = \frac{\frac{\partial u(t_c,T_h)}{\partial T_c}v(t_c,T_h) - \frac{\partial v(t_c,T_h)}{\partial T_c}u(t_c,T_h)}{[v(t_c,T_h)]^2} = 0 \tag{29}$$

This leads to the rearrangement of the equation as:

$$\begin{aligned} &R(T_c, T_h)\left\{\int_0^{T_c} R(t_c, T_h)dt_c + R(T_c, T_h)\bar{M}_{pc} + [1-(R(T_c, T_h))]\bar{M}_{cc}\right\} \\ &-\left\{R(T_c, T_h) - \mathscr{F}_{\mathscr{C}}(T_c, T_h)\bar{M}_{pc} + \mathscr{F}_{\mathscr{C}}(T_c, T_h)\bar{M}_{cc}\right\}\int_0^{T_c} R(t_c, T_h)dt_c = 0 \end{aligned} \tag{30}$$

From Eq. (30) we get:

$$\frac{\bar{M}_{cc}}{\bar{M}_{cc}-\bar{M}_{pc}} = R(T_c, T_h) + \frac{\mathscr{F}_{\mathscr{C}}(T_c, T_h)}{R(T_c, T_h)}\int_0^{T_c} R(t_c, T_h)dt_c \tag{31}$$

Eq. (31) describes that with any given value of T_h in Fig. 2, the value of the optimum value of T_c can be obtained with known values of $\bar{M}_{cc}$ and $\bar{M}_{pc}$. Function $\mathscr{F}_{\mathscr{C}}(t_c, T_h)$ represents the probability density function of the projected distribution function, with FC t_c as variable, by the expression of the reliability surface at vertical plane at $t_h = T_h$. This probability density function of the projected function can be analytically deduced, and are given in Table 4 based on the four candidate copula models.

Similarly, given any fixed value of T_c on the t_c axis, the projected reliability distribution by vertical plane at $t_c = T_c$ is $R(T_c, t_h)$. The determination of T_h by maximum availability is:

$$A_h = \frac{\int_0^{T_h} R(T_c, t_h)dt_c}{\int_0^{T_h} R(T_c, t_h)dt_h + R(T_c, t_h)\bar{M}_{ph} + [1-(R(T_c, t_h))]\bar{M}_{ch}} \tag{32}$$

with further deduction procedure leads to:

$$\frac{\bar{M}_{ch}}{\bar{M}_{ch}-\bar{M}_{ph}} = R(T_c, t_h) + \frac{\mathscr{F}_{\mathscr{H}}(T_c, t_h)}{R(T_c, t_h)}\int_0^{T_h} R(T_c, t_h)dt_h \tag{33}$$

In Eq. (33) the function $\mathscr{F}_{\mathscr{H}}(T_c, t_h)$ represents the probability density function of the projected distribution function on the t_h axis, similar to $\mathscr{F}_{\mathscr{C}}(t_c, T_h)$. The expression of the probability density functions for the four copula candidates on the t_h axis are also given in Table 4.

One common term for all the $\mathscr{F}_{\mathscr{H}}(T_c, t_h)$ and $\mathscr{F}_{\mathscr{C}}(t_c, T_h)$ in Table 4 is the differentiation of the marginal distribution functions $\frac{dF_1(t_c)}{dt_c}$ and $\frac{dF_2(t_h)}{dt_h}$. As the marginal distribution is selected from the target reliability functions from Eqs. (4) to (7). We can therefore obtain the differentiation functions of the target functions, as shown in Table 5.

The functions in Section 2.2.3.1 provides the analytical formats of the terms in need to solve the optimum overhaul interval in a bivariate background. This means that given any value T_h on the t_h axis, upon known values of $\bar{M}_{cc}$ and $\bar{M}_{pc}$, the value of the most optimum T_c can be obtained. Symmetrically, given any value T_c on the t_c axis, upon known values of $\bar{M}_{ch}$ and $\bar{M}_{ph}$, the most optimum T_h can be obtained. This lead to the iteration algorithm in Section 2.2.3.2.

2.2.3.2 Iteration algorithm With the key calculations in Section 2.2.3.1, the iteration algorithm is presented in Section 2.2.3.2.

The converged value of *Reliability* from Algorithm 2 sets the threshold of maintenance interval based on the reliability surface approach, the threshold is thus represented in the reliability contour according to the format of the copula function from Table 3, with the value of r in all candidate functions as the converged *Reliability* value.

Table 5
Differentiation of the four target reliability functions.

Target reliability function	Differentiation of reliability function
GEV reliability function	$-\frac{1}{\sigma}\left[1+\xi\left(\frac{t-\mu}{\sigma}\right)\right]^{-(\xi+1)/\xi} exp\left\{-\left[1+\xi\left(\frac{t-\mu}{\sigma}\right)\right]^{-1/\xi}\right\}$
Weibull reliability function	$-\frac{\xi}{\sigma}\left(\frac{t}{\sigma}\right)^{\xi-1} exp\left[-(\frac{t}{\sigma})^{\xi}\right]$
Gumbel reliability function	$\frac{1}{\sigma} exp\left[-\frac{t-\mu}{\sigma}+exp\left(-\frac{t-\mu}{\sigma}\right)\right]$
Normal reliability function	$\frac{1}{\sigma\sqrt{2\pi}} exp\left[-\frac{1}{2}\left(\frac{t-\mu}{\sigma}\right)^2\right]$

Algorithm 2 Iteration Algorithm

procedure Define Function
  ASSIGN $\bar{M}_{cc}, \bar{M}_{pc}, \bar{M}_{ch}, \bar{M}_{pc}$ ▷ Obtain maintenance time
  INPUT $\xi_c, \sigma_c, \mu_c, \xi_h, \sigma_h, \mu_h, \phi$ ▷ Input parameters
  $R(t_c, t_h) \leftarrow R(t_c, t_h, \xi_c, \sigma_c, \mu_c, \xi_h, \sigma_h, \mu_h, \phi)$ ▷ Copula reliability model, equation (12)
  $F_C(t_c, t_h) \leftarrow F_C(t_c, t_h, \xi_c, \sigma_c, \mu_c, \xi_h, \sigma_h, \mu_h, \phi)$ ▷ F_C candidate function from Table 4 and Table 5
  $F_H(t_c, t_h) \leftarrow F_H(t_c, t_h, \xi_c, \sigma_c, \mu_c, \xi_h, \sigma_h, \mu_h, \phi)$ ▷ F_H candidate function from Table 4 and Table 5
end procedure
procedure Iteration
  for $i \leftarrow 1, n$ **do**
    $T_{hour}[1] \leftarrow T_{hour}[initial]$ ▷ Assign initial value on the t_h axis within domain $[0, 1]$
    $T_{cycle}[i] \leftarrow$ SOLVE $\frac{\bar{M}_{cc}}{\bar{M}_{cc}-\bar{M}_{pc}} = R(T_c, T_{hour}[i]) + \frac{\mathscr{F}_{\mathscr{C}}(T_c, T_{hour}[i])}{R(T_c, T_{hour}[i])} \int_0^{T_c} R(t_c, T_{hour}[i]) dt_c$
    $T_{hour}[i] \leftarrow$ SOLVE $\frac{\bar{M}_{ch}}{\bar{M}_{ch}-\bar{M}_{ph}} = R(T_{cycle}[i], T_h) + \frac{\mathscr{F}_{\mathscr{C}}(T_{cycle}[i], T_h)}{R(T_{cycle}[i], T_h)} \int_0^{T_h} R(T_{cycle}[i], t_h) dt_h$
    $Capability[i] \leftarrow \sqrt{(T_{cycle}[i])^2 + (T_{hour}[i])^2}$
    $Reliability[i] \leftarrow R(T_{cycle}[i], T_{hour}[i])$
  end for ▷ Loop until $Capability$ and $Reliability$ value converge
end procedure

2.3. Fleet operation life resilient monitoring

The establishment of the reliability contour as well as the determination of the reliability threshold for overhaul interval timeline enables the capability for both monitoring single engine health condition, as well as monitoring the resilience for all the engines within a fleet. The capability of monitoring individual engine usage is beneficial for flight planning in order to use the maximum capability of an engine in both the FH capability and the FC capability, or in another explanation, to maximize the RUL. The fleet resilience is beneficial to minimize the disruptions of engine overhaul activities, by estimating the lead time needed for maintenance activities in guaranteeing the availability of sufficient healthy aircraft engines at any time window to fulfill the planned flight arrangements for all airline operators. We consider both the individual engine usage monitoring and the fleet resilient monitoring scenarios separately.

2.3.1. Engine usage trajectory

Here we propose and define 'usage trajectory' in the aviation industry for propulsion systems. Consider an engine is currently at a state (T_c, T_h) on the reliability contour, meaning the engine has used a total of cycles T_c on its FC capability and a total of hours of T_h on its FH capability. Assume the airplane equipped with this engine is arranged with n continuous flights, each with a duration of hour $h_i, i \in \mathbb{Z}, i \in [1, n]$, note that this value of h_i is normalized as all other time measurements in the present study. Each flight with duration of hour h_i cost the engine FC capability with one cycle, and after normalization it is represented by c. The engine usage trajectory on the reliability contour with axis of (t_c, t_h) from its current state (T_c, T_h) is thus a series of discrete points represented as:

$$(T_c, T_h) \rightarrow (T_c + c, T_h + h_1) \rightarrow (T_c + 2c, T_h + h_1 + h_2) \rightarrow \cdots \rightarrow (T_c + nc, T_h + \sum_{i=1}^{n} h_i) \tag{34}$$

with the connected routes among each pair of adjacent discrete points on the reliability contour defined as the engine usage trajectory. The associated reliability values for the engine usage at each flight are:

$$R(T_c, T_h) \rightarrow R(T_c + c, T_h + h_1) \rightarrow R(T_c + 2c, T_h + h_1 + h_2) \rightarrow \cdots \rightarrow R(T_c + nc, T_h + \sum_{i=1}^{n} h_i) \tag{35}$$

where $R(t_c, t_h)$ is the copula model from Eq. (12). This enables an estimation of the RUL of such engine within one overhaul cycle at any time point. The estimation of the RUL is directly associated with the flight routes operated by the airline. Assume the longest route the airline operates under the capability of the airplanes with this engine model has a duration in hours of h_{max}, and the shortest route has a duration in hours of h_{min}, these two routes also mean they have the highest and the lowest hour to cycle ratios. Take a random state of the engine from the trajectory in Eqs. (34) and (35), location $(T_c + kc, T_h + \sum_{i=1}^{k} h_i)$, the associated reliability estimation as $R(T_c + kc, T_h + \sum_{i=1}^{k} h_i)$, as shown in Fig. 3.

From Fig. 3, the engine moved from $State_{k-1}((T_c + (k-1)c, T_h + \sum_{i=1}^{k-1} h_i, R(T_c + (k-1)c, T_h + \sum_{i=1}^{k-1} h_i)))$ to $State_k((T_c + kc, T_h + \sum_{i=1}^{k} h_i, R(T_c + kc, T_h + \sum_{i=1}^{k} h_i)))$ after one flight. The maximum RUL in the FH capability exists when the airplane is arranged for the flight with the longest duration in

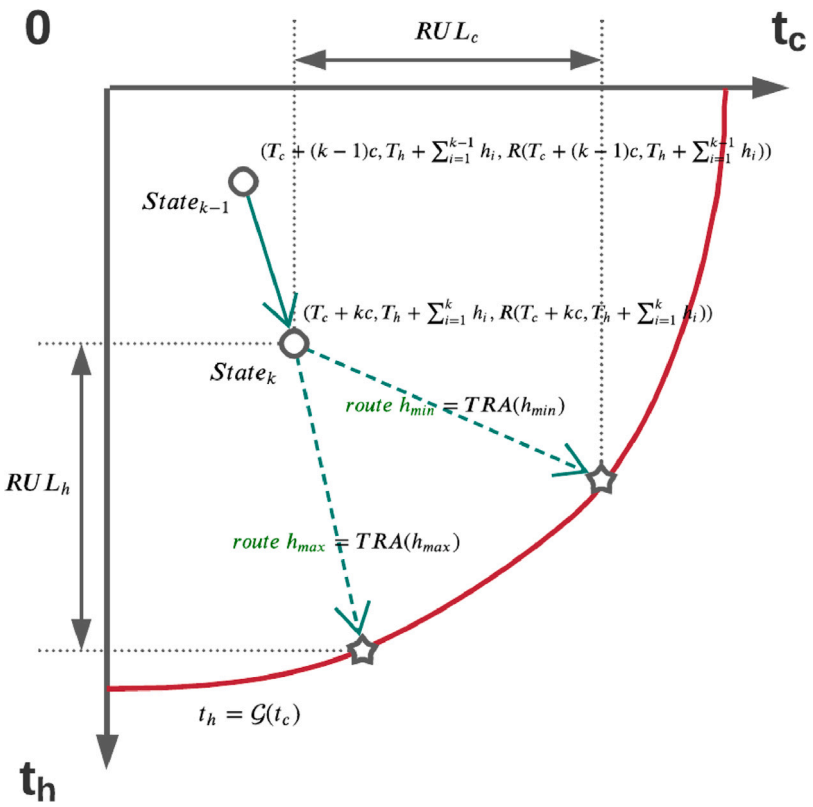

Fig. 3. Single engine RUL by usage trajectory monitoring.

hours, following trajectory function $TRA(h_{max})$, until reaching the overhaul threshold of $t_h = \mathcal{G}(t_c)$ from Table 3. Similarly, the maximum RUL in the FC capability exists when the airplane is arranged for flight with the shorted duration in hours, following the trajectory function $TRA(h_{min})$, until reaching the overhaul threshold. The trajectory functions of $TRA(h_{max})$ and $TRA(h_{min})$ on the reliability contour with t_h as the dependent variable and t_c as the independent variable at $State_k$ are given as:

$$TRA(h_{max}) : t_h = \frac{h_{max}}{c} t_c + T_h + \sum_{i=1}^{k} h_i - \frac{h_{max}}{c}(T_c + kc) \tag{36}$$

and

$$TRA(h_{min}) : t_h = \frac{h_{min}}{c} t_c + T_h + \sum_{i=1}^{k} h_i - \frac{h_{min}}{c}(T_c + kc) \tag{37}$$

The upper limit of the RUL in FH along the t_h axis RUL_h, and the upper limit of the RUL in FC along the t_c axis RUL_c, are obtained by solving the set of equations with Eqs. (36), (37) and the overhaul threshold function on the reliability contour $t_h = \mathcal{G}(t_c)$. As the overhaul threshold on the reliability contour in the present study has the potential candidate format of 4 copula models, each copula model contains two marginal distributions with 4 potential formats, that is in total 64 potential function formats of $\mathcal{G}(t_c)$. For example, the solution to the estimation of maximum RUL in FH, assuming $\mathcal{G}(t_c)$ is based on the Gumbel copula, and both marginal distributions follows the GEV distribution is the solution of Eqs. (36), and (38) as:

$$t_h = \mu_h + \frac{\sigma_h}{\xi_h}\left(\left(-log\left(1 - \left(exp\left(-\left((-log\ r)^{\phi} - \left(-log\left(1 - e^{-\left(1+\xi_c\left(\frac{t_c-\mu_c}{\sigma_c}\right)\right)^{-1/\xi_c}}\right)\right)^{\phi}\right)^{1/\phi}\right)\right)\right)^{-\xi_h} - 1\right) \tag{38}$$

The solution of t_c is therefore obtainable by solving the equation:

$$\mu_h + \frac{\sigma_h}{\xi_h}\left(\left(-log\left(1 - \left(exp\left(-\left((-log\ r)^{\phi} - \left(-log\left(1 - e^{-\left(1+\xi_c\left(\frac{t_c-\mu_c}{\sigma_c}\right)\right)^{-1/\xi_c}}\right)\right)^{\phi}\right)^{1/\phi}\right)\right)\right)^{-\xi_h} - 1\right) = \frac{h_{max}}{c} t_c + T_h + \sum_{i=1}^{k} h_i - \frac{h_{max}}{c}(T_c + kc) \tag{39}$$

Among all the 64 potential function formats of $\mathcal{G}(t_c)$, the estimation of RUL depends on the solving of complex equations like the example in Eq. (39). The analytical solution varies in format and can be difficult to deduce. The numerical approach on equation solving is popular for its versatility. Therefore, we propose an algorithm for RUL estimation on the aircraft engine reliability contour, which is a generic solution to all the 64 variations of equations.

Table 6
An airline operator operating m commercial routes with airplanes equipped with the same model of aircraft engines.

Route	Duration of trip (normalized hour)	Count of normalized cycle	Demand in duration D
Route 1	h_1	c	d_1
Route 2	h_2	c	d_2
Route 3	h_3	c	d_3
⋮	⋮	⋮	⋮
Route m	h_m	c	d_m

Table 7
Fleet usage states at any time point.

Airplane number	Pair of engine number	Usage state on reliability contour
Airplane 1	Engine pair 1	(T_{c1}, T_{h1})
Airplane 2	Engine pair 2	(T_{c2}, T_{h2})
Airplane 3	Engine pair 3	(T_{c3}, T_{h3})
⋮	⋮	⋮
Airplane n	Engine pair n	(T_{cn}, T_{hn})

Define function (40) here, and the numerical solution is provided in Algorithm Algorithm 3.

$$\mathscr{F}(t) = \frac{h}{c}t + T_h + \sum_{i=1}^{k} h_i - \frac{h}{c}(T_c + kc) - \mathscr{G}(t) \; where \; h \in [h_{min}, h_{max}] \; and \; t = t_c \tag{40}$$

Algorithm 3 RUL Estimation

procedure ITERATION
- $t[0] = t$
- $t[1] = t[0] + 0.01$ ▷ input two initial values of equation solution
- **for** $q \leftarrow 1, n$ **do**
  - $t[q+1] \leftarrow t[q] - (t[q] - t[q-1]) \frac{\mathscr{F}(t[q])}{\mathscr{F}(t[q]) - \mathscr{F}(t[q-1])}$ ▷ Iteration step
- **end for** ▷ Loop until $t[q]$ converge
- OBTAIN $t_c[k]$ ▷ Converged value of $t[q]$ at state k
- $t_h[k] \leftarrow \frac{h}{c}t_c[k] + T_h + \sum_{i=1}^{k} h_i - \frac{h}{c}(T_c + kc)$
- $RUL_c[k] \leftarrow t_c[k] - (T_c + kc)$
- $RUL_h[k] \leftarrow t_h[k] - (T_h + \sum_{i=1}^{k} h_i)$ ▷ RUL at state k

end procedure

2.3.2. Fleet resilience

Fleet resilience is an extended concept in the present study based on the single engine RUL monitoring, by an integration of engine usage trajectories mapping on the reliability contour as a fleet. The fleet resilient monitoring is vital to avoid disruptions in business operations for airline operators, as the total capability of engines determines the confidence on the airline to fulfill all the planned flight routes in any future time window. Assume an airline owns a fleet of n airplanes equipped with the same models of aircraft engines is operating m commercial routes, as shown in Table 6. In Table 6 the 'Demand in duration D' column considers the number of flights to be scheduled among destinations within calendar days of D.

In order to fulfill the scheduled routes in duration D, the fleet must has a RUL capability in hours with $(\sum_{i=1}^{m} d_i h_i)$ and the RUL capability in cycles with $(c \sum_{i=1}^{m} d_i)$. The fleet resilient monitoring estimates the total capability of the n pairs of aircraft engines with varies usage states and usage trajectories, on the fleet's ability to fulfill the minimum RUL requirement at any given duration in the future. This estimation allows the operator and the aircraft engine providers to plan on the scenarios with either sufficient RUL exists or there is insufficient RUL, in order to minimize the disturbance to the fleet operations. Assume the n-airplane fleet equip with the aircraft engines, each pair of engines are at the same usage state, and the usage states are different among all pairs of engines, as shown in Table 7.

The RUL of the fleet of engines at the engine states in Table 7 is calculated based on the weighted average of hour/cycle ratio within duration D:

$$\bar{h_D} = \frac{\sum_{i=1}^{m} d_i h_i}{\sum_{i=1}^{m} d_i} \tag{41}$$

For demonstration purpose, Fig. 4 demonstrates a fleet of 3 pairs of engines on the reliability contour with current engine state. The RUL as a fleet is estimated via Algorithm Algorithm 3 on each pair of engine following the weighted hour/cycle ratio trajectory.

The RUL with the FH is therefore $\sum_{i=1}^{n} RUL_{h_i}$ and with the FC is $\sum_{i=1}^{n} RUL_{c_i}$. These two values are compared with the demanded RUL capability in hours with $(\sum_{i=1}^{m} d_i h_i)$ and the RUL capability in cycles with $(c \sum_{i=1}^{m} d_i)$. With both the sufficient RUL and insufficient RUL scenarios, either there is sufficient RUL in fulfilling the flights demand, or there is insufficient RUL in fulfilling the demand. These two scenarios will be discussed accompanied with numerical examples in the results and discussion section.

3. Results & discussion

In this section, we provide a case study based on one model of engine currently in service commercially, and with 101 unplanned run-to-failure cases identified in the maintenance logbook which led to the overhaul of these engines. In this paper we name this model of civil aircraft engine

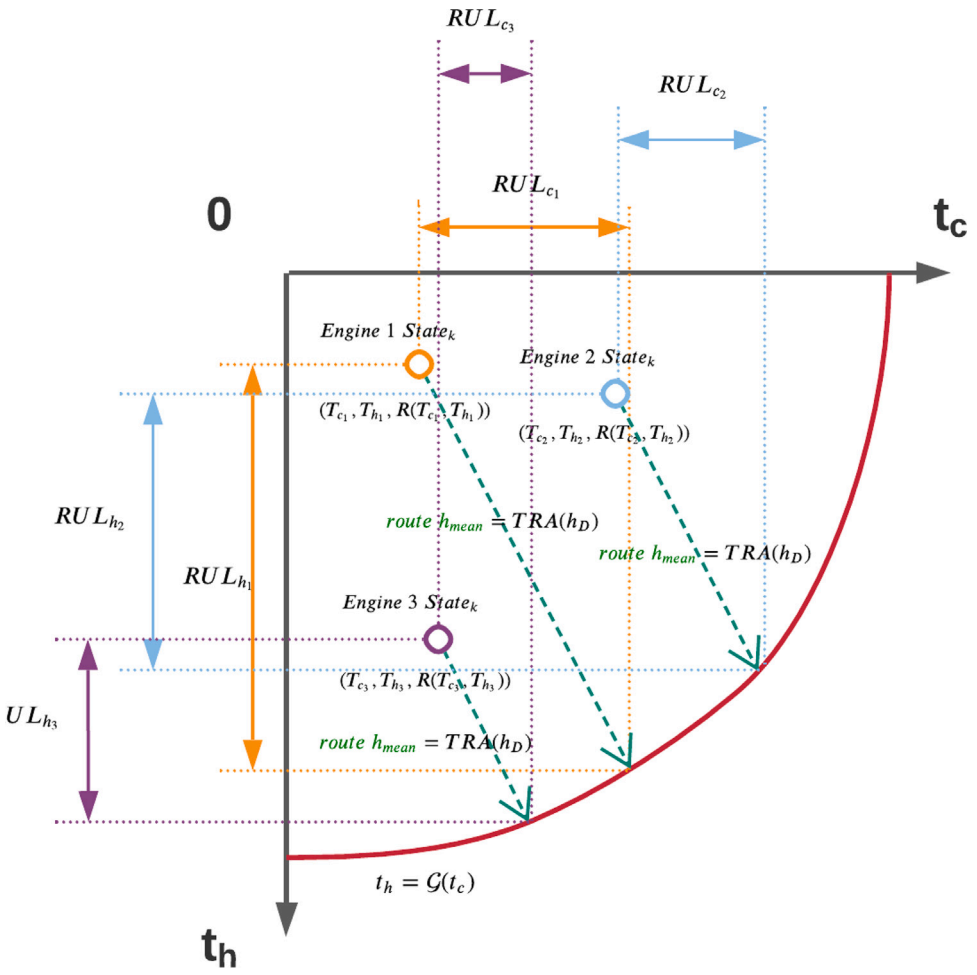

Fig. 4. Fleet resilience calculation demonstration.

Table 8
Maintenance records after normalization for engine model Ω.

Label	Product model	Model number	Normalized hour	Normalized cycle	Capability
1	Ω	1510	0.1175	0.1092	0.1604
2	Ω	1458	0.1433	0.0970	0.1730
3	Ω	1457	0.2020	0.2486	0.3203
4	Ω	1549	0.1080	0.1085	0.1531
5	Ω	1531	0.1435	0.1721	0.2241
...	...	...	...	...	...
101	Ω	1483	1.0000	0.8554	1.3160

as Model Ω. In Table 8 we provide the format of the dataset after the normalization procedure according to Eq. (1), the capability of the engine is also included calculated by Eq. (2). The model number in Table 8 represent the individual engine identification within the same model fleet Ω. A histogram representation on the data distribution for model Ω in both FH before overhaul and the FC before overhaul is provided in Fig. 5. It can be observed from Fig. 5 that the most frequent count on FH is between 0.3 and 0.4, while the most frequent count on FC is between 0.5 and 0.6.

Following the initial data processing as shown in Table 8, the usage of capability by each engine in the fleet is calculated, ranked and performed survival analysis on the estimation of fleet reliability of the engine model. This section is further divided into: A. the deduction of the reliability contour of engine model Ω. B. the determination of overhaul interval and end-of-life threshold. C. Engine usage trajectory mapping and estimation of fleet resilience.

3.1. Reliability contour

3.1.1. Marginal distribution determination

By survival analysis from Eq. (3), the capability of engine usage before overhaul is calculated for the entire sample population. The population of dataset therefore contains three dimensions of information, (FC, FH, Reliability) = $(t_{ci}, t_{h_i}, R(C_i))$. The three dimensional calculated information is shown in Fig. 6(a), along with the marginal distribution created by the projection of the reliability values on the FH axis t_h and the FC axis t_c. The marginal distribution is then fitted with the four potential targeted reliability functions from Eqs. (4) to (7), where the best functions to

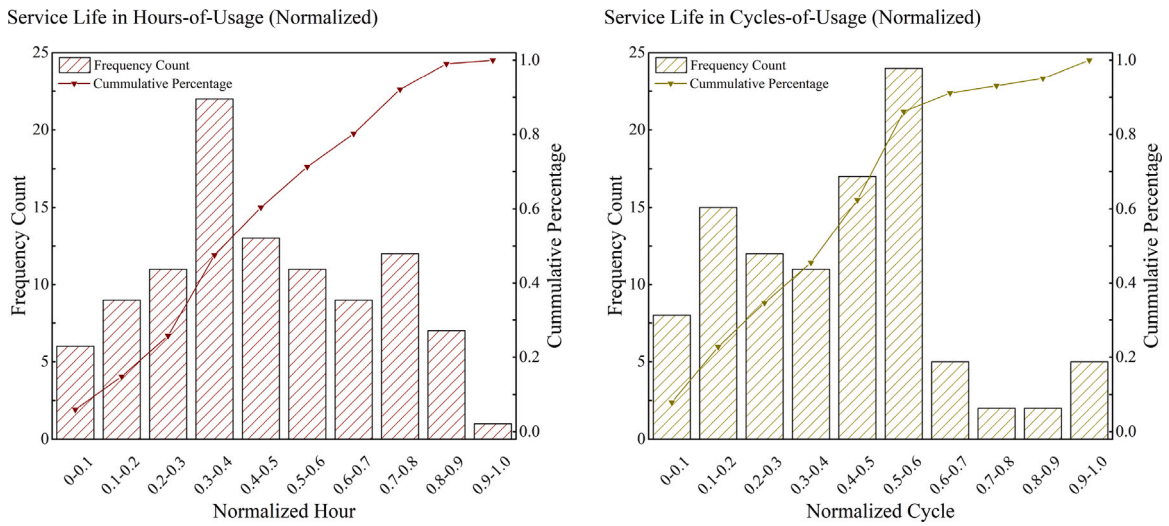

Fig. 5. Operation record distribution of engine model Ω.

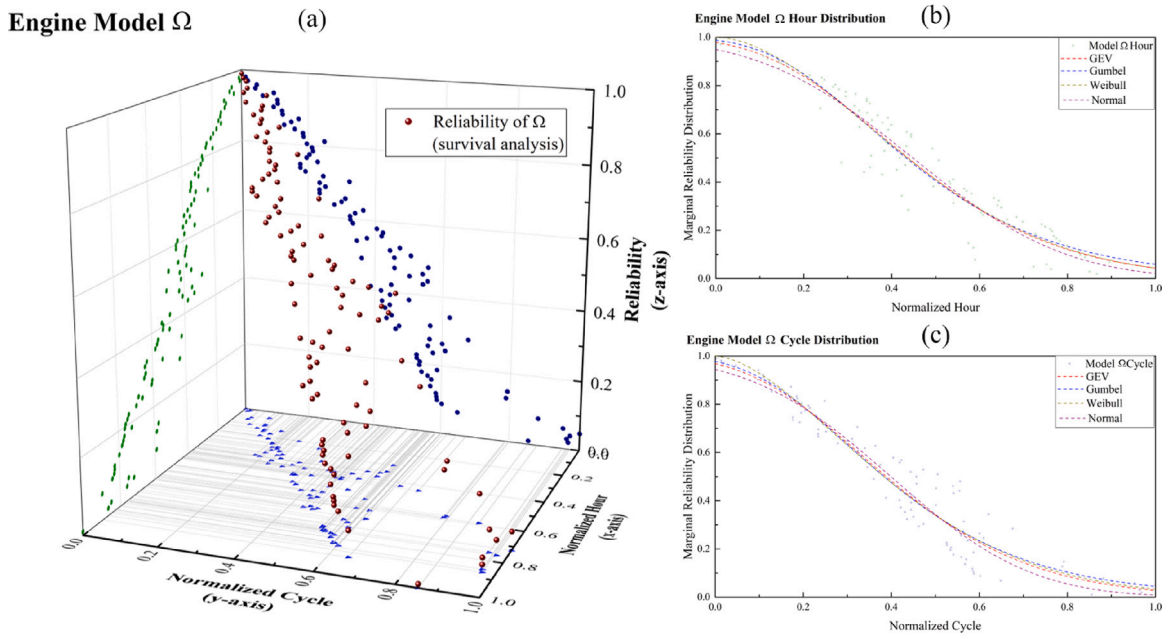

Fig. 6. (a) Reliability 3-dimensional scatter of engine model Ω (b)(c) Marginal distribution and reliability model fitting for engine model Ω.

describe the marginal distribution on both axis are determined, also shown in Fig. 6(b) and (c). The distribution choices are based on the coefficient of determination $\mathbb{R}^2$. The comparison of the candidate marginal reliability model is provided in Table 9.

It can be observed from both Fig. 6 and Table 9, that the best reliability model to describe the marginal distribution of the fleet after survival analysis is the GEV distribution. The parameters determined for the reliability models on both time axis as well as the $\mathbb{R}^2$ values for both axis of the best choice are shaded in light gray color, while the $\mathbb{R}^2$ values are in red color. It is worth noticing that the GEV distribution format has the advantage of being a three parameter determined distribution, while the other three candidates are two parameter controlled distributions. The second best choice for the FH reliability marginal distribution is the Gumbel distribution, while the second best choice for the FC reliability marginal distribution is the Weibull distribution. The two second best choices are shaded in pink color, and the associated $\mathbb{R}^2$ values are in blue color. This lead to the potential combinations of marginal distribution reliability model to develop the integrated copula model in the next step as: 1. Best choice: (FH, FC) = (GEV Reliability Model, GEV Reliability Model) 2. All two-parameter controlled reliability model choice: (FH, FC) = (Gumbel Reliability Model, Weibull Reliability Model). Both of the mentioned choices are carried forward for the copula model development.

3.1.2. Copula reliability surface model

With the marginal distributions obtained, this section describes the selection of a copula model which integrates both of the marginal distributions and forms a mathematical model describing the combined contributions of the FH and FC towards the civil aircraft engine reliability.

Table 9
Marginal distribution format selection on two time scales for the fleet reliability of engine model Ω.

Distribution	Engine model Ω			
	Hour	$\mathbb{R}^2_{Hour}$	Cycle	$\mathbb{R}^2_{Cycle}$
Weibull	$\sigma = 0.533$ $\xi = 1.817$	0.9254	$\sigma = 0.478$ $\xi = 1.660$	0.9236
Gumbel	$\sigma = 0.233$ $\mu = 0.347$	0.9258	$\sigma = 0.226$ $\mu = 0.0.301$	0.9234
Normal	$\sigma = 0.273$ $\mu = 0.448$	0.9248	$\sigma = 0.251$ $\mu = 0.399$	0.9207
GEV	$\sigma = 0.243$ $\mu = 0.350$ $\xi = -0.101$	0.9268	$\sigma = 0.232$ $\mu = 0.305$ $\xi = -0.100$	0.9243

Table 10
$\mathbb{R}^2$ for four copula model candidates with parametric ϕ calculation approach.

Copula model	Marginal distribution (GEV, GEV)	Marginal distribution (Gumbel, Weibull)
Gumbel	0.8947	0.8930
Clayton	0.8821	0.8780
Independence	0.5325	0.5274
Frank	0.7580	0.7538

Table 11
Comparison of parametric and non-parametric approach for copula model selection.

Marginal distribution	Clayton Copula			Gumbel Copula		
	$\mathbb{R}^2_{parametric}$	$\mathbb{R}^2_{non-parametric}$	Improvement	$\mathbb{R}^2_{parametric}$	$\mathbb{R}^2_{non-parametric}$	Improvement
(GEV, GEV)	0.8821	0.9068	2.8%	0.8947	0.9116	1.9%
(Gumbel, Weibull)	0.8780	0.9050	3.1%	0.8930	0.9097	1.9%

With the four potential copula models given in Eqs. (8)–(11), the key in determining the optimum copula model is the estimation of the association measurement parameter ϕ. From Tables 1 and 2, conventionally ϕ can be estimated via the calculation of the Kendall's τ. This is the parametric approach and is generally applied when the relationship between the two variables are simple. The parametric approach is performed on the two marginal distribution combinations, and the results are given in Table 10. It can be observed from Table 10 that the Gumbel copula model achieves the highest values of $\mathbb{R}^2$, shaded in the gray color. The values obtained via the Clayton copula model is not far behind from the Gumbel copula. The Independence copula and the Frank copula, however, is not as well performed, hence they are eliminated at this stage as the candidate copula choices.

On the contrary, when the relationship between the two variables are complex, for example the failure modes contribution by the FH and the FC towards the quantified reliability assessment of the civil aircraft engines, the parametric approach may not perform well describing the combined effects of both variables. Therefore we proposed the non-parametric approach on estimating the parameter ϕ via Monte-Carlo sampling as mentioned in Algorithm 1, in order to provide better modeling performance without over-fitting. A comparison between the parametric approach and the non-parametric approach for copula model is shown in Table 11, on both the Gumbel copula model and the Clayton copula model.

As observed from Table 11, the non-parametric approach improves the accuracy of the copula model on describing the distribution of data points in space, ranging from 1.9% to 3.1%. The best copula model, as shown in the yellow color cell in Table 11, is the marginal distribution combination of (GEV distribution, GEV distribution), applying the Gumbel copula and utilizing the non-parametric approach for the association measurement parameter ϕ calculation. This model provides an $\mathbb{R}^2$ value of 0.9116. The ϕ value associated with this choice of copula model is 5.82. Therefore, the copula model that describes the data point distribution in three-dimensional space from Fig. 6(a) is given here, this is regarded as the reliability surface function describing the performance of the civil aircraft engine being researched in this paper:

$$F_{\Omega} = exp\left(-\left(\left(-log\left(1-e^{-\left(1-0.101\left(\frac{t_h-0.350}{0.243}\right)\right)^{-1/-0.101}}\right)^{5.82}\right)+\left(-log\left(1-e^{-\left(1-0.100\left(\frac{t_c-0.305}{0.232}\right)\right)^{-1/-0.100}}\right)^{5.82}\right)\right)^{1/5.82}\right) \tag{42}$$

From Table 3 and Eqs. (13) to (15) and Eq. (54), the deduced reliability surface copula model is transferable into a reliability contour map. With a model in Eq. (42), for a Gumbel copula with ϕ value of 5.82, the marginal distribution for cycles of usage as GEV distribution format with parameters of $(\sigma = 0.232, \mu = 0.305, \xi = -0.100)$, marginal distribution for hours of usage as GEV distribution format with parameters of $(\sigma = 0.243, \mu = 0.350, \xi = -0.101)$, the reliability contour lines within the plane coordinates of (t_c, t_h) for all reliability values r within the domain $[0, 1]$ is given as:

$$t_h = 0.350 - \frac{0.243}{0.101}\left(\left(-log\left(1-\left(exp\left(-\left((-logr)^{5.82}-\left(-log\left(1-e^{-\left(1-0.100\left(\frac{t_c-0.305}{0.232}\right)\right)^{-1/-0.100}}\right)\right)^{5.82}\right)^{1/5.82}\right)\right)^{0.101}\right)\right)-1\right) \tag{43}$$

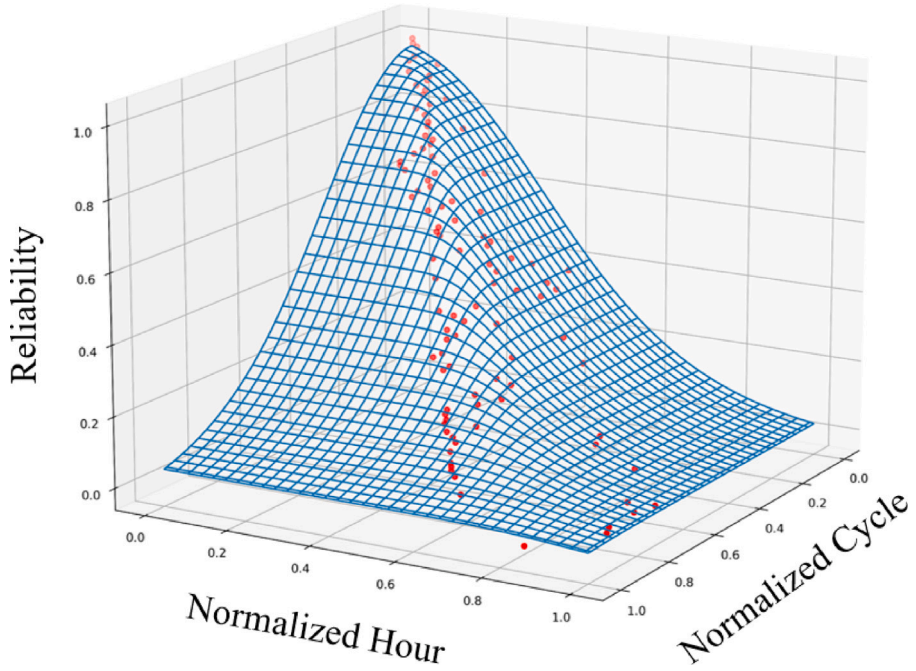

Fig. 7. Developed reliability surface model.

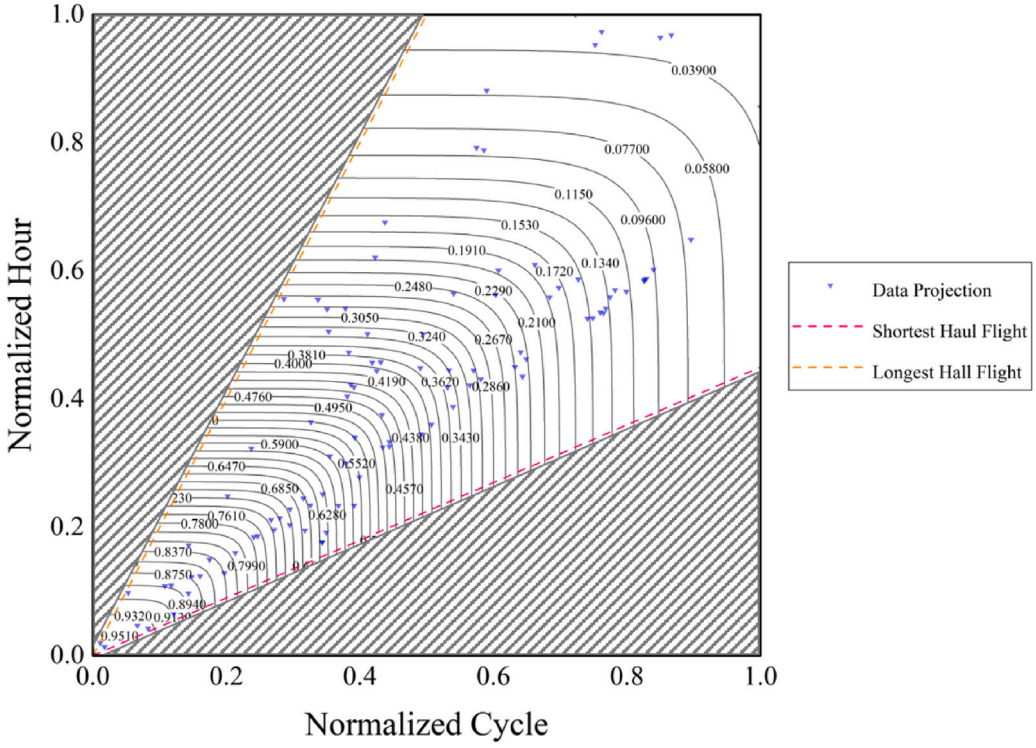

Fig. 8. Reliability contour with data points projected on the (t_c, t_h) plane.

From Eq. (43) it can be observed that with any fixed value of reliability r, a relationship function between t_h and the variable of t_c can be obtained. The result of both the reliability surface from Eq. (51) is shown in Fig. 7. The reliability contour map deduction from Eq. (52) are shown in Fig. 8. Fig. 8 are partly shaded, which emphasizes the effective zone of such a reliability contour map, the shaded area are ineffective zones, the boundaries of the zones are set by the longest haul and shortest haul of the operating flights, which provides the largest and smallest hour/cycle ratio of the fleet population.

3.2. Overhaul interval determination

With the obtaining of the reliability surface model as well as the reliability contour transforming the reliability surface into the two dimensional plane, the model is further utilized to determine the overhaul intervals. An overhaul decision is made when the reliability of the engine is lower than a threshold, or failures are detected where engines cannot continue to safely operate hence require full refurbishment. In order to obtain the overhaul interval based on the optimization of maximum availability of the aircraft engine fleet, it is important to obtain four values regarding the maintenance duration, the loss of engine operating time in cycles by preventive maintenance $\bar{M}_{pc}$, the loss of engine operating time in hours by preventive maintenance $\bar{M}_{ph}$, the loss of engine operating time in cycles by corrective maintenance $\bar{M}_{cc}$ and the loss of engine operating time in hours by corrective maintenance $\bar{M}_{ch}$. Assume each corrective maintenance takes a duration of t_{cor} calendar days and a preventive maintenance takes a duration of t_{pre} calendar days, on average for each calendar day that an engine goes through overhaul, it costs the engine to lose $\bar{t_{cycle}}$ of flights, which is $\bar{t_c}$ of cycles, similarly, each calendar day loss costs the engine $\bar{t_{hour}}$ of flying hours. This lead to the disturbance of engine operation by preventive maintenance or corrective maintenance as:

$$\begin{cases} \bar{M}_{pc} = t_{pre} \times \bar{t_{cycle}} \\ \bar{M}_{ph} = t_{pre} \times \bar{t_{hour}} \\ \bar{M}_{cc} = t_{cor} \times \bar{t_{cycle}} \\ \bar{M}_{ch} = t_{cor} \times \bar{t_{hour}} \end{cases} \tag{44}$$

By substituting the loss of operation time defined in set of Eqs. (44) into Eq. (21), we obtain the deduced availability model for the fleet of engine model Ω in the present study as:

$$\begin{cases} W = \dfrac{\sqrt{\left[\int_0^{T_c} R(t_c,T_h)dt_c\right]^2 + \left[\int_0^{T_h} R(T_c,t_h)dt_h\right]^2}}{\sqrt{\left[\int_0^{T_c} R(t_c,T_h)dt_c\right]^2 + \left[\int_0^{T_h} R(T_c,t_h)dt_h\right]^2} + \sqrt{\begin{matrix}\{R(T_c,T_h)\times t_{pre}\times \bar{t_{cycle}} + [1-R(T_c,T_h)]\times t_{cor}\times \bar{t_{cycle}}\}^2 + \\ \{R(T_c,T_h)\times t_{pre}\times \bar{t_{hour}} + [1-R(T_c,T_h)]\times t_{cor}\times \bar{t_{hour}}\}^2\end{matrix}}} \\ where \\ R(t_c,T_h) = exp\left(-\left(\left(-log\left(1-e^{-\left(1-0.101\left(\frac{T_h-0.350}{0.243}\right)\right)^{-1/-0.101}}\right)^{5.82}\right) + \left(-log\left(1-e^{-\left(1-0.100\left(\frac{t_c-0.305}{0.232}\right)\right)^{-1/-0.100}}\right)^{5.82}\right)\right)^{1/5.82}\right) \\ and \\ R(T_c,t_h) = exp\left(-\left(\left(-log\left(1-e^{-\left(1-0.101\left(\frac{t_h-0.350}{0.243}\right)\right)^{-1/-0.101}}\right)^{5.82}\right) + \left(-log\left(1-e^{-\left(1-0.100\left(\frac{T_c-0.305}{0.232}\right)\right)^{-1/-0.100}}\right)^{5.82}\right)\right)^{1/5.82}\right) \\ and \\ R(T_c,T_h) = exp\left(-\left(\left(-log\left(1-e^{-\left(1-0.101\left(\frac{T_h-0.350}{0.243}\right)\right)^{-1/-0.101}}\right)^{5.82}\right) + \left(-log\left(1-e^{-\left(1-0.100\left(\frac{T_c-0.305}{0.232}\right)\right)^{-1/-0.100}}\right)^{5.82}\right)\right)^{1/5.82}\right) \end{cases} \tag{45}$$

In order to determine the threshold of reliability where the combination of (T_c, T_h) enables the maximum expectation of availability for the fleet of aircraft engines, the key is to solve Eqs. (26) and (27) on both time scales. The terms and functions in both equations are given in Eq. (45). As introduced in Section 2.2.3, in order to solve the set of complex equations, the proposed iteration Algorithm 2 is applied. Here we provide a numerical simulation to test the stability and robustness of this iteration algorithm on equation solving. From Algorithm 2, it can be seen that the solution of equations on both time scales requires the calculation of ratios:

$$\begin{cases} \dfrac{\bar{M}_{cc}}{\bar{M}_{cc}-\bar{M}_{pc}} = \dfrac{t_{cor}\times \bar{t_{cycle}}}{t_{cor}\times \bar{t_{cycle}} - t_{pre}\times \bar{t_{cycle}}} = \dfrac{t_{cor}}{t_{cor}-t_{pre}} \\ \dfrac{\bar{M}_{ch}}{\bar{M}_{ch}-\bar{M}_{ph}} = \dfrac{t_{cor}\times \bar{t_{hour}}}{t_{cor}\times \bar{t_{hour}} - t_{pre}\times \bar{t_{hour}}} = \dfrac{t_{cor}}{t_{cor}-t_{pre}} \end{cases} \tag{46}$$

Eq. (46) simplifies the equation on parameter value demands, both equations in Algorithm 2 require the ratio of corrective maintenance time duration and the preventive maintenance time duration, regardless of the time units. This ratio can be regarded as a penalty factor for performing the corrective and the preventive maintenance. In the modern engineering industry, even with the fastest reaction on unplanned corrective maintenance, with the time lost responding to emergencies, lead time of parts order and shipping, extra time in diagnosing faults while equipment is not working, the penalty of such corrective maintenance can be around three times higher than the preventive maintenance [30]. For numerical simulation we test the ratio r_{cp} between corrective maintenance and preventive maintenance of 1.5 to 4, with a 0.5 increment. Furthermore, based on the developed reliability surface model, with Gumbel copula model, both t_c and t_h marginal distributions follow the GEV distribution and parameters

determined, the following functions are obtained:

$$
\begin{cases}
R(t_c,t_h) = R(t_c,\ t_h,\ \xi_c,\ \sigma_c,\ \mu_c,\ \xi_h,\ \sigma_h,\ \mu_h,\ \phi) = R(t_c,\ t_h,\ -0.100,\ 0.232,\ 0.305,\ -0.101,\ 0.243,\ 0.350,\ 5.82) \\
= exp\left(-\left(\left(-log\left(1-e^{-\left(1-0.101\left(\frac{t_h-0.350}{0.243}\right)\right)^{-1/-0.101}}\right)^{5.82}\right)+\left(-log\left(1-e^{-\left(1-0.100\left(\frac{t_c-0.305}{0.232}\right)\right)^{-1/-0.100}}\right)^{5.82}\right)\right)^{1/5.82}\right) \\
\\
\mathscr{F}_{\mathscr{C}}(t_c,T_h) = \mathscr{F}_{\mathscr{C}}(t_c,\ T_h,\ \xi_c,\ \sigma_c,\ \mu_c,\ \xi_h,\ \sigma_h,\ \mu_h,\ \phi) = \mathscr{F}_{\mathscr{C}}(t_c,\ T_h,\ -0.100,\ 0.232,\ 0.305,\ -0.101,\ 0.243,\ 0.350,\ 5.82) \\
= -\left\{exp\left\{-[(-logF_1(t_c))^{5.82}+(-logF_2(T_h))^{5.82}]^{1/5.82}\right\}\right\}[(-logF_1(t_c))^{5.82}+(-logF_2(T_h))^{5.82}]^{1/5.82-1}\frac{(-logF_1(t_c))^{5.82-1}}{F_1(t_c)}\frac{dF_1(t_c)}{dt_c} \\
\\
\mathscr{F}_{\mathscr{H}}(T_c,t_h) = \mathscr{F}_{\mathscr{H}}(T_c,\ t_h,\ \xi_c,\ \sigma_c,\ \mu_c,\ \xi_h,\ \sigma_h,\ \mu_h,\ \phi) = \mathscr{F}_{\mathscr{H}}(T_c,\ t_h,\ -0.100,\ 0.232,\ 0.305,\ -0.101,\ 0.243,\ 0.350,\ 5.82) \\
= -\left\{exp\left\{-[(-logF_1(T_c))^{5.82}+(-logF_2(t_h))^{5.82}]^{1/5.82}\right\}\right\}[(-logF_1(T_c))^{5.82}+(-logF_2(t_h))^{5.82}]^{1/5.82-1}\frac{(-logF_2(t_h))^{5.82-1}}{F_2(t_h)}\frac{dF_2(t_h)}{dt_h} \\
\\
where \\
\\
F_1(t_c) = 1-e^{-\left(1-0.100\left(\frac{t_c-0.305}{0.232}\right)\right)^{-1/-0.100}} \\
\\
F_2(t_h) = 1-e^{-\left(1-0.101\left(\frac{t_h-0.350}{0.243}\right)\right)^{-1/-0.101}} \\
\\
\frac{dF_1(t_c)}{dt_c} = -\frac{1}{0.232}\left[1-0.100\left(\frac{t_c-0.305}{0.232}\right)\right]^{-(-0.100+1)/-0.100} exp\left\{-\left[1-0.100\left(\frac{t_c-0.305}{0.232}\right)\right]^{-1/-0.100}\right\} \\
\\
\frac{dF_2(t_h)}{dt_h} = -\frac{1}{0.243}\left[1-0.101\left(\frac{t_h-0.350}{0.243}\right)\right]^{-(-0.101+1)/-0.101} exp\left\{-\left[1-0.101\left(\frac{t_h-0.350}{0.243}\right)\right]^{-1/-0.101}\right\}
\end{cases}
\tag{47}
$$

With each simulation, an initial value on the t_h axis is assigned to the variable t_h as T_{hour}. For each ratio r_{cp} of corrective maintenance and preventive maintenance, 5 different values are assigned by random numbers within the domain of t_h $[0, 1]$. The number of iterations which enables Algorithm 2 to converge and achieve stability, as well the reliability value obtained by Algorithm 2 are provided in Table 12.

Table 12 proves that under different r_{cp} ratio, and each ratio with randomly assigned initial values of T_{hour}, the iteration algorithm converges after a number of iterations and stabilize at all combinations of input values, providing the reliability value which is the threshold of overhaul interval for a fleet of aircraft engines. This threshold determination enables the maximum availability of the fleet. The stabilizing convergence by iteration Algorithm 2 is also provided in Fig. 9. Fig. 9 shows the convergence pattern of every combinations of ratio r_{cp} and initial value of T_{hour} for variable on the t_h coordinate. Generally, within 50 iterations, Algorithm 2 can achieve stability and convergence, which leads to the solution of the complex set of Eqs. (26) and (27). The reliability threshold value obtained via the solution of the equations determines the reliability contour line as the threshold for aircraft engine operation monitoring. The determined threshold contour line for all the simulated r_{cp} ratios from Table 12 are shown in Fig. 10. It can be observed that, with the ratio r_{cp} of corrective maintenance and preventive maintenance duration increases, which can be interpreted as the penalty for unplanned maintenance activities, the determined overhaul interval reliability threshold gets larger. This is a reasonable results, as the more severe of consequence unplanned maintenance activities cause, the maintenance interval should be shorter in order to guarantee a higher reliability of aircraft engines as a fleet.

In this paper the r_{cp} ratio of 2 is used to demonstrate the usage trajectory monitoring as well as the fleet resilient monitoring in the next section. The 'Overhaul interval threshold reliability contour line' function when $r_{cp} = 2$ is given here in Eq. (48), and this contour line function is the blue threshold as plotted in Fig. 11 under 'Overhaul Threshold ratio = 2':

$$
t_h = 0.350-\frac{0.243}{0.101}\left(\left(-log\left(1-\left(exp\left(-\left((-log\,(0.220))^{5.82}-\left(-log\left(1-e^{-\left(1-0.100\left(\frac{t_c-0.305}{0.232}\right)\right)^{-1/-0.100}}\right)\right)^{5.82}\right)^{1/5.82}\right)\right)^{0.101}\right)\right)-1\right) \tag{48}
$$

3.3. Fleet operation life resilient monitoring

In this section, based on the overhaul threshold determined by $r_{cp} = 2$ with its associated contour line function, we provide two applications of the reliability contour: One being health monitoring of single civil aircraft engine, and the other one for monitoring the entire fleet. These applications are possible by recording the continuous usage, mapping the usage trajectory on the reliability contour, and a continuous calculation of the remaining useful in both time scale measurements towards the determined threshold of overhaul interval, which is considered as the end-of-life for a healthy engine within one overhaul cycle. The engine going through a full-refurbishment overhaul will reset its monitoring start point to the original 100% reliability pint $(0.0, 0.0)$ in a reliability contour, and restart its usage trajectory monitoring. With this set-up, as one brand new engine typically goes through 3 to 4 full-refurbishment overhauls through-out its life cycle, by recording down the number that the usage is set back to the original point, the anticipated RUL of an engine towards its end of life cycle (or the time to retire) is also obtainable. We divide this section of results with two case studies, one focusing on the usage and reliability monitoring of a single aircraft engine, and the other one on an entire fleet of the studied aircraft engine.

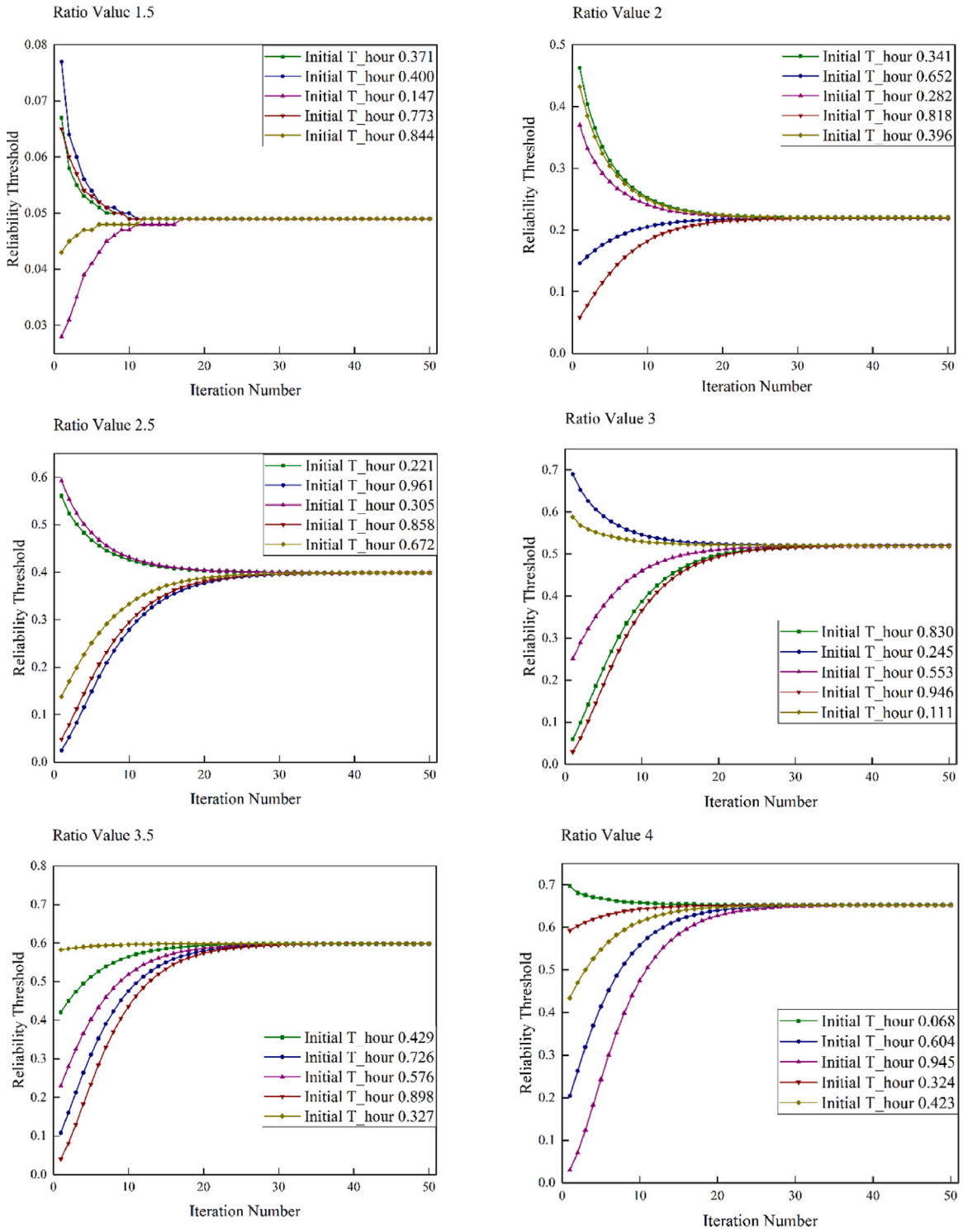

Fig. 9. Algorithm 2 convergence with combinations of ratio r_{cp} and random initial values of T_{hour}.

3.3.1. Single engine health monitoring

In order to perform the single engine health monitoring by referring to its usage and declination in reliability, it is important to track each individual flight, particularly the duration of each flight. The duration of flight is within an effective zone as defined previously. As seen in Fig. 11, the effective zone is the un-shaded area which is bonded by the longest haul flight and the shortest haul flight that the airplanes equipped with this model of engine is capable to operate. In Fig. 11, the shortest haul flight being operated by engine model Ω is with a 3.1 h/cycle ratio and the longest haul flight is with a 15.4 h/cycle ratio. An airline operator AO manages 30 different routes of flights according to the capability of the engine model Ω with distinctive duration in flying hours, meaning the airplanes equipped with engine model Ω has the capability to fly all the 30 routes. The details of the 30 flight routes are given in Appendix A. As the reliability contour developed in this paper considers only the

Table 12
Comparison of parametric and non-parametric approach for copula model selection.

Ratio r_{cp}	Initial T_{hour}	Stabilized iteration number	Converge reliability value
1.5	0.371	17	0.049
	0.400	19	
	0.147	18	
	0.773	18	
	0.844	13	
2	0.341	35	0.220
	0.652	30	
	0.282	32	
	0.818	35	
	0.396	34	
2.5	0.221	33	0.399
	0.961	41	
	0.305	34	
	0.858	41	
	0.672	38	
3	0.830	40	0.520
	0.245	32	
	0.553	36	
	0.946	41	
	0.111	28	
3.5	0.429	29	0.598
	0.726	36	
	0.576	34	
	0.898	38	
	0.327	16	
4	0.068	21	0.653
	0.604	38	
	0.945	41	
	0.324	27	
	0.423	33	

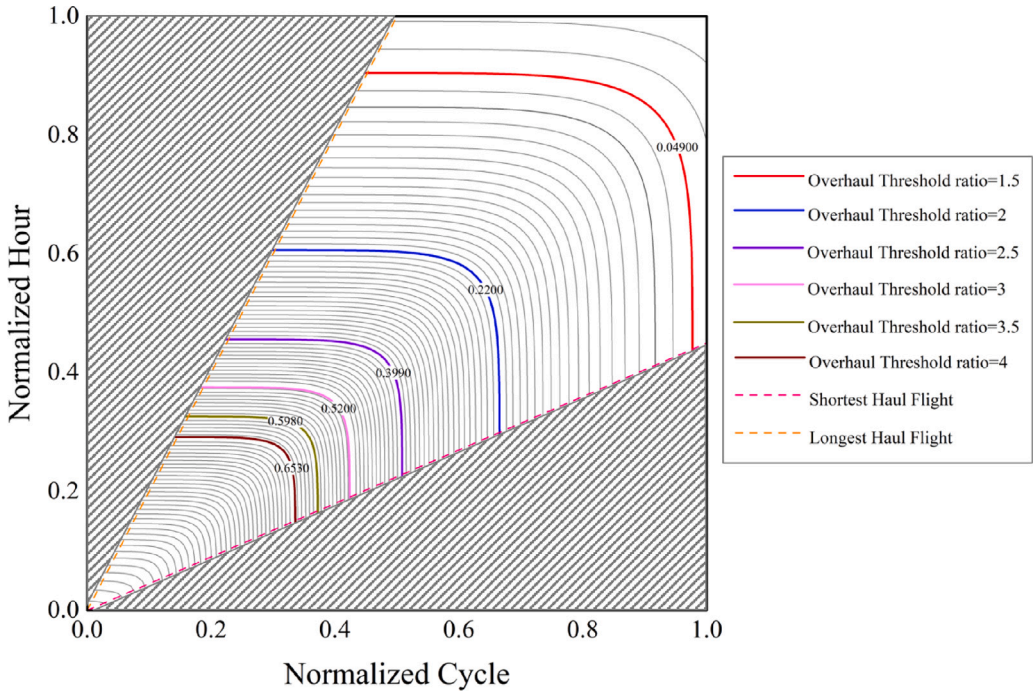

Fig. 10. Overhaul interval threshold with simulated corrective maintenance to preventive maintenance ratio r_{cp}.

operational time of the engines, therefore the geological locations of these flights are not control factors. The estimation of the engine capability to fulfill the planned flight schedule is important for airline operators, as it result in both avoiding disturbance in the aviation operation, as well as the successful planning and arrangement of maintenance activities with sufficient lead time for crucial spare parts. Let aircraft A_1 belonging to airline operator AO, which equipped with a pair of engine model Ω and went into service from brand new, currently has a usage history in normalized hours and normalized cycles as $(T_c, T_h) = (0.473, 0.556)$. This usage history maps the aircraft engine on the reliability contour for currently estimated

Table 13
Usage trajectory coordinates and RUL calculation for aircraft engine in 14 calendar days forward planning.

Calendar day	Engine state	Contour coordinate (t_c, t_h)	Reliability	RUL hours (min, max)	RUL Cycle (min, max)
Start	k	(0.47300, 0.55600)	0.26900	(0.02242, 0.09962)	(0.04981, 0.22145)
1	k + 1	(0.47327, 0.55646)	0.26850	(0.02232, 0.09916)	(0.04958, 0.22043)
2	k + 2	(0.47354, 0.55692)	0.26799	(0.02221, 0.09870)	(0.04935, 0.21941)
3	k + 3	(0.47385, 0.55707)	0.26781	(0.02218, 0.09856)	(0.04928, 0.21907)
4	k + 4	(0.47416, 0.55722)	0.26763	(0.02214, 0.09840)	(0.04920, 0.21873)
5	k + 5	(0.47440, 0.55737)	0.26745	(0.02211, 0.09826)	(0.04913, 0.21840)
6	k + 6	(0.47463, 0.55753)	0.26727	(0.02208, 0.09810)	(0.04905, 0.21806)
7	k + 7	(0.47485, 0.55768)	0.26709	(0.02204, 0.09794)	(0.04897, 0.21772)
8	k + 8	(0.47508, 0.55783)	0.26691	(0.02201, 0.09780)	(0.04890, 0.21738)
9	k + 9	(0.47538, 0.55798)	0.26673	(0.02197, 0.09764)	(0.04882, 0.21704)
10	k + 10	(0.47564, 0.55814)	0.26655	(0.02194, 0.09750)	(0.04875, 0.21670)
11	k + 11	(0.47596, 0.55844)	0.26620	(0.02187, 0.09718)	(0.04859, 0.21602)
12	k + 12	(0.47626, 0.55890)	0.26570	(0.02177, 0.09672)	(0.04836, 0.21501)
13	k + 13	(0.47664, 0.55920)	0.26536	(0.02170, 0.09642)	(0.04821, 0.21433)
14	k + 14	(0.47697, 0.55951)	0.26501	(0.02163, 0.09612)	(0.04806, 0.21365)

reliability as $r_k = exp\left(-\left(\left(-log\left(1-e^{-\left(1-0.101\left(\frac{0.556-0.350}{0.243}\right)\right)^{-1/-0.101}}\right)^{5.82}\right)+\left(-log\left(1-e^{-\left(1-0.100\left(\frac{0.473-0.305}{0.232}\right)\right)^{-1/-0.100}}\right)^{5.82}\right)\right)^{1/5.82}\right) = 0.3105$, r_k represents that the engine health is currently at state k. The planned flight route in the next two calendar week, or fourteen calendar days, is provided in Appendix B. Each calendar day with the flight arrangement shifts the engine health state with one forward, e.g., state $k+1$ for calendar day 1, state $k+2$ for calendar day 2 and so on. Each state with its accumulated normalized hours of usage and accumulated normalized cycles of usage is mapped on the associated reliability contour, and the shifting of states on the reliability contour map is the usage trajectory of the studied aircraft engine in this example. The health state k until the planned two calendar weeks with fourteen days of increment in health states with their associated values is provided in Table 13. Furthermore, the health-state-shifting mapped on the reliability contour is presented in Fig. 11. The calculation of RUL with the lower and upper boundaries for both remaining life in hours of usage (RUL_h) and in cycles of usage (RUL_c), for example, at state k, with the determined overhaul interval threshold from Eq. (48), is to solve the set of equations:

$$\begin{cases} 0.350-\frac{0.243}{0.101}\left(\left(-log\left(1-\left(exp\left(-\left((-log\,(0.220))^{5.82}-\left(-log\left(1-e^{-\left(1-0.100\left(\frac{t_{cmin}-0.305}{0.232}\right)\right)^{-1/-0.100}}\right)\right)^{5.82}\right)^{1/5.82}\right)\right)\right)\right)^{0.101}-1\right) \\ = 15.4t_{cmin}-8.0132 \\ 0.350-\frac{0.243}{0.101}\left(\left(-log\left(1-\left(exp\left(-\left((-log\,(0.220))^{5.82}-\left(-log\left(1-e^{-\left(1-0.100\left(\frac{t_{cmax}-0.305}{0.232}\right)\right)^{-1/-0.100}}\right)\right)^{5.82}\right)^{1/5.82}\right)\right)\right)\right)^{0.101}-1\right) \\ = 3.1t_{cmax}-1.1688 \\ t_{hmax} = 15.4t_{cmin}-8.0132 \\ t_{hmin} = 3.1t_{cmax}-1.1688 \end{cases} \tag{49}$$

The set of equations is associated with the longest haul and shortest haul of the flights operated by the airlines, where the longest haul flight, with the largest hour/cycle ratio, determines the upper boundary of RUL_h and the lower boundary of RUL_c, while the shortest haul flight with the smallest hour/cycle ratio determines the lower boundary of RUL_c and the upper boundary of RUL_h. Applying Algorithm Algorithm 3 introduced, the results for Eq. (58) are $RUL_h(min, max) = (0.02242, 0.09962)$ and $RUL_c(min, max) = (0.04981, 0.22145)$. With the same calculation procedures, the estimation of the future 14 calendar days on engine health states, including the estimated reliability value of each state, the upper and lower boundaries of the RUL in both hours and cycles are shown in Table 13. The associated usage trajectory monitoring of the 14 engine health states as well as the current engine state k is further shown in Fig. 11. The routes where the reliability of the engine declines on the reliability contour map can be clearly observed in this figure, with both the trajectory in the full scale contour map and the zoom in view of the usage trajectory.

3.3.2. Fleet resilient monitoring

We have demonstrated the capability of the reliability contour which can be used to monitor the engine health state, to estimate the quantified reliability level in advance, and to estimate the remaining useful lives for both the hours of usage and the cycles of usage for flight planning. In addition to this, the entire fleet can be monitored and planned in the same fashion. It is especially beneficial for both the airline operators and the engine providers' maintenance sector to understand the performance of the fleets in general. Take an example that the airline operator *AO* operates the 30 flight routes with a fleet of 50 airplanes, each plane with a pair of model Ω aircraft engines. The weekly demand and arrangement of the 30 flight routes with their associated total normalized flying hours and flying cycles are given in Appendix C. Weekly demand here is regarded as one change of state, where state $k'+1$ represent the fleet state in one calendar week. The current reliability state k' for the fleet of engines is provided in Appendix D.

From Appendix D, at state k', the fleet has a resilience 13.7372 of RUL in hours, and a resilience of 15.0958 RUL in cycles. The total capability of the fleet is sufficient for the next weekly flight scheduling, comparing to the weekly demand of 0.01596 normalized hours and 0.01754 cycles.

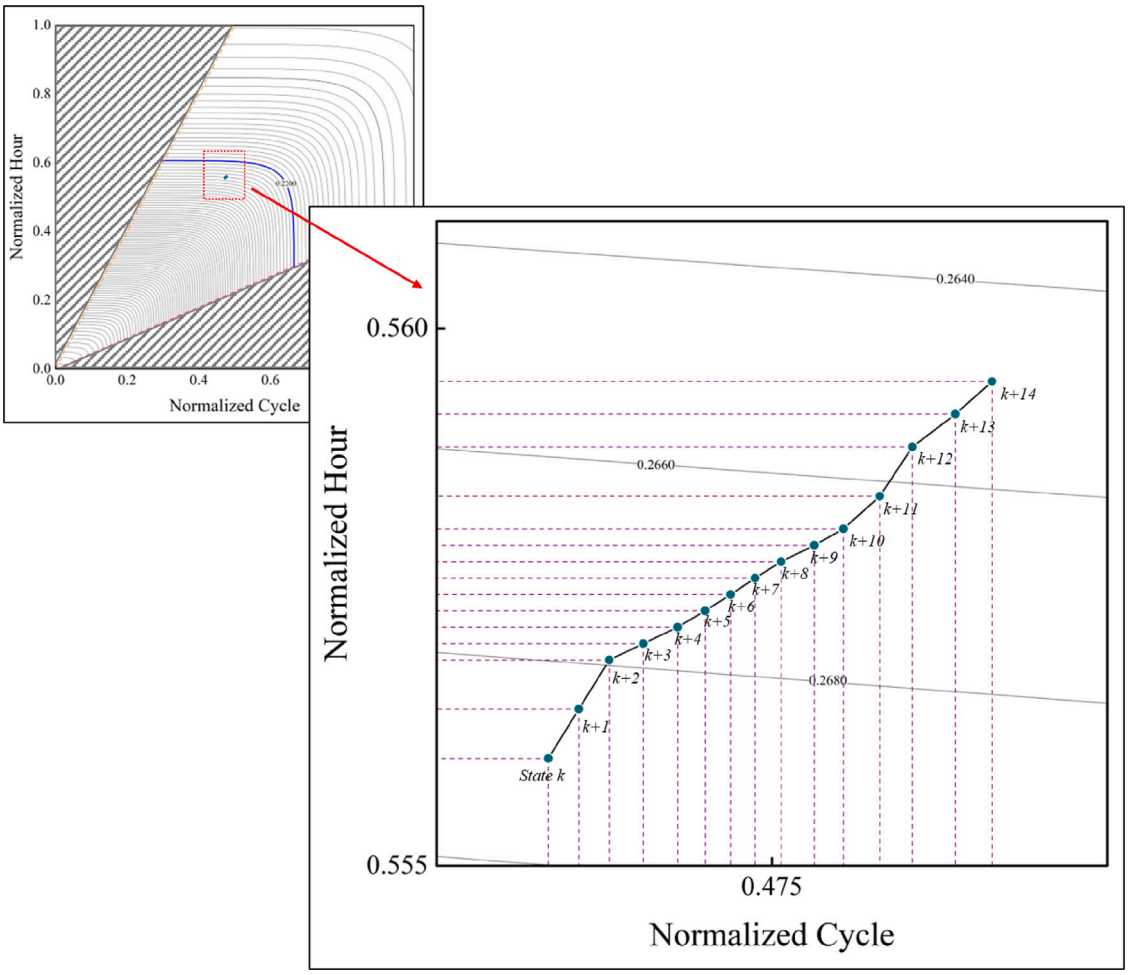

Fig. 11. Usage trajectory monitoring of the engine states in 14 calendar days on the reliability contour.

The total resilience of the fleet is updated with fixed intervals, and the approximate time window when the fleet resilience is not sufficient to fulfill the demanded flight arrangements can be obtained. This is valuable information on maintenance planning as well as the arrangements of flight routes to avoid potential disturbance of operations.

4. Conclusion

This paper focused on a type of highly valuable and reliability-demanding transportation systems, the civil aircraft engines. The paper analyzed the life-cycle performance, quantified reliability estimation, definition of the end-of-life, as well as creating a statistical-based visualization tool for health monitoring and RUL estimation for the aviation industry. For a highly complex engineering system as such, it suffers multiple types of deterioration which lead to multiple failure modes. This paper utilized the real life run-to-failure operation data for a fleet of the engines with the same model and design, provided by our industrial partner. Based on this dataset which contains the overhaul timing information in both the FH and FC, we proposed a novel copula reliability model combining the two time scales and formed a joint evaluation of the engine capabilities based on the dual measurements. The model is further deduced into the reliability contour map, and is used as a foundation to define the end-of-service-cycle in the dual-time-scale background, providing a threshold for the calculation of RUL of each aircraft engine in a fleet. Furthermore, combining the reliability contour map and the threshold determination, a way to monitor the history of the engine usage through its life cycle is proposed, which is a visualization tool for fleet planning and maintenance planning towards a fleet of the civil aircraft engines.

The paper has made three major contributions to the aviation industry and transportation research field:

(1) The paper propose a novel model for the performance evaluation and reliability estimation for a fleet of the civil aircraft engines. The present study discovers that, for the fleet of engines as use cases in the paper, the Gumbel copula with both the marginal distributions for the FH and FC as GEV distributions, along with the association measurement parameter ϕ estimated via the non-parametric Monte-Carlo simulation based approach, describes the reliability of the civil aircraft engines the best. The copula reliability model is further developed into the reliability contour map to transform the three-dimensional model into two-dimensional representation, for the convenience of application in real life for the aviation industry.

(2) Based on the deduced reliability contour map, the end-of-service-cycle threshold is defined and calculated in order to maximize the availability of the aircraft engine fleet, which in another explanation, is the time between overhaul of the aircraft engines. The threshold calculation requires the information of time cost on the preventive maintenance and the corrective maintenance in the aviation industry.

In order to obtain the quantified reliability threshold for overhaul intervals based on the copula reliability model, an iteration algorithm is proposed and tested on multiple numerically simulated combinations. The testing results proved the algorithm's robustness and stability towards convergence in the complex equation solving capability. The obtained end-of-service-cycle threshold is further used as the target life for the estimation of RUL, for each of the aircraft engine in the fleet at any given accumulated usage state.

(3) With the combination of the proposed copula reliability model, reliability contour map and the determination of the overhaul interval threshold, the quantified reliability value and the RUL in FH remaining and the FC of each aircraft engine is obtainable at any given time point of the engine's life-cycle. Therefore, the integrated solution is proposed as a visualization health monitoring tool for the civil aircraft engine fleet. The usage trajectory of each individual engine is mapped over the reliability contour map of the fleet based on the duration of each flight and the count of the number of flights in service. At every health state, the RUL is a direct quantified decision support information advising the best flight route arrangement for the operators, and the overhaul planning for engine manufacturers and maintenance service providers. Considering multiple engine state mapped on the reliability contour map, the paper also proposed a solution for estimating the fleet resilience of engines belonging to the same model, which is a valuable quantified output for fleet management and decision-making.

The authors' next stage work will focus on the optimization of flight routes by airline operators who own a fleet of airplanes equipped with the same model of engines, based on the variety of flight duration and demands, referring to the copula reliability model and the overhaul threshold schedules, in order to estimate the fleet resilience and a combined capability of the fleets on fulfilling annual flying hour targets. Another follow up on the research topic is the determination of multi-level maintenance executions based on the copula reliability model, on the perfect maintenance, imperfect maintenance, on-wing and off-wing minimal repair timeline thresholds of such civil aircraft engines, on both maximizing the availability and minimizing the cost of their life cycle services.

CRediT authorship contribution statement

Hang Zhou: Conceptualization, Methodology, Software, Validation, Formal analysis, Data curation, Writing – original draft, Writing – review & editing, Visualization. **Maryam Farsi:** Methodology, Writing – original draft, Writing – review & editing, Project administration, Funding acquisition. **Andrew Harrison:** Conceptualization, Resources, Supervision, Project administration, Funding acquisition. **Ajith Kumar Parlikad:** Conceptualization, Methodology, Resources, Writing – review & editing, Supervision, Project administration. **Alexandra Brintrup:** Resources, Project administration, Funding acquisition.

Declaration of competing interest

The authors declare that they have no known competing financial interests or personal relationships that could have appeared to influence the work reported in this paper.

Data availability

The data that has been used is confidential.

Acknowledgments

This research was funded by Aerospace Technology Institute and Innovate UK, the UK's innovation funding agency, through the "Digitally Optimised Through-Life Engineering Services" project (113174). The first author would also like to thank St Edmund's College, University of Cambridge, for the fellowship, which provided support throughout this research.

Appendix A. Flight routes details operated by airline operator AO

Flight route	Flight duration (h)	Normalized hours per flight	Normalized cycles per flight
1	11.8	0.000233891	0.000152532
2	3.1	6.15275E−05	0.000152532
3	6.5	0.000129131	0.000152532
4	3.7	7.27991E−05	0.000152532
5	4.3	8.52398E−05	0.000152532
6	13.2	0.000262554	0.000152532
7	11.6	0.000231153	0.000152532
8	7.0	0.000138939	0.000152532
9	15.4	0.000305653	0.000152532
10	3.5	6.99366E−05	0.000152532

11	8.5	0.000168636	0.000152532
12	7.8	0.000154675	0.000152532
13	12.5	0.000248409	0.000152532
14	12.9	0.000255656	0.000152532
15	5.4	0.000107148	0.000152532
16	9.1	0.000181091	0.000152532
17	8.6	0.000170306	0.000152532
18	11.0	0.000219309	0.000152532
19	11.8	0.000234701	0.000152532
20	12.4	0.000245765	0.000152532
21	6.5	0.000128912	0.000152532
22	11.5	0.00022746	0.000152532
23	11.2	0.000221453	0.000152532
24	5.1	0.000101225	0.000152532
25	4.6	9.05778E−05	0.000152532
26	9.2	0.000183191	0.000152532
27	14.9	0.000295825	0.000152532
28	7.3	0.000144624	0.000152532
29	10.3	0.000204406	0.000152532
30	5.9	0.000116166	0.000152532

Appendix B. Planned flight routes in calendar days

Calendar day	Planned routes	Flying hour by day	Flying cycle by day	Normalized hour	Normalized cycle
1	3 + 4 + 10	13.7	3	0.000271912	0.000457596
2	9	15.4	1	0.000305653	0.000152532
3	9	15.4	1	0.000305653	0.000152532
4	11 + 12	16.3	2	0.000323515	0.000305064
5	20	12.4	1	0.00024611	0.000152532
6	22	11.5	1	0.000228247	0.000152532
7	18	11	1	0.000218323	0.000152532
8	19	11.8	1	0.000234201	0.000152532
9	26 + 28	16.5	2	0.000327485	0.000305064
10	27	14.9	1	0.000295729	0.000152532
11	6	13.2	1	0.000261988	0.000152532
12	2 + 21 + 24	14.7	3	0.000291759	0.000457596
13	8 + 20	19.4	2	0.000385043	0.000305064
14	14	12.9	1	0.000256034	0.000152532

Appendix C. Weekly flight demands for all flight routes

Route	Duration (h)	Number of flights	Total normalized hours	Total normalized cycles
1	11.8	1	0.000233891	0.000152532
2	3.1	10	0.000615275	0.00152532
3	6.5	4	0.000516525	0.000610128
4	3.7	6	0.000436794	0.000915192
5	4.3	6	0.000511439	0.000915192
6	13.2	1	0.000262554	0.000152532
7	11.6	2	0.000462305	0.000305064
8	7.0	4	0.000555758	0.000610128
9	15.4	1	0.000305653	0.000152532
10	3.5	10	0.000699366	0.00152532
11	8.5	4	0.000674544	0.000610128
12	7.8	4	0.000618702	0.000610128
13	12.5	1	0.000248409	0.000152532
14	12.9	1	0.000255656	0.000152532
15	5.4	6	0.000642887	0.000915192
16	9.1	4	0.000724365	0.000610128
17	8.6	4	0.000681225	0.000610128

18	11.0	4	0.000877235	0.000610128
19	11.8	2	0.000469402	0.000305064
20	12.4	1	0.000245765	0.000152532
21	6.5	2	0.000257824	0.000305064
22	11.5	4	0.00090984	0.000610128
23	11.2	2	0.000442907	0.000305064
24	5.1	4	0.0004049	0.000610128
25	4.6	4	0.000362311	0.000610128
26	9.2	6	0.001099144	0.000915192
27	14.9	1	0.000295825	0.000152532
28	7.3	4	0.000578497	0.000610128
29	10.3	2	0.000408812	0.000305064
30	5.9	10	0.001161656	0.00152532
Sum			0.015959466	0.017541184

Appendix D. Fleet of engines at state k'

Aircraft label	Reliability contour coordinate	RUL hours	RUL cycles
1	(0.0427, 0.0584)	0.5972	0.6563
2	(0.0559, 0.0946)	0.5611	0.6165
3	(0.1486, 0.1312)	0.5245	0.5763
4	(0.1305, 0.1650)	0.0693	0.0762
5	(0.1121, 0.1833)	0.4723	0.5191
6	(0.1362, 0.2206)	0.0642	0.0705
7	(0.2203, 0.2428)	0.4128	0.4537
8	(0.2163, 0.2466)	0.4091	0.4496
9	(0.2902, 0.1659)	0.4898	0.5382
10	(0.1864, 0.2816)	0.0185	0.0203
11	(0.2521, 0.2457)	0.4099	0.4505
12	(0.2640, 0.2375)	0.4181	0.4595
13	(0.2774, 0.2397)	0.4159	0.4571
14	(0.3000, 0.2785)	0.3771	0.4144
15	(0.3608, 0.2669)	0.3888	0.4272
16	(0.2271, 0.3880)	0.2676	0.2941
17	(0.3503, 0.3055)	0.3502	0.3848
18	(0.2233, 0.4201)	0.2355	0.2587
19	(0.2843, 0.3821)	0.2736	0.3006
20	(0.3151, 0.3669)	0.2887	0.3173
21	(0.4399, 0.2076)	0.4480	0.4923
22	(0.3371, 0.3604)	0.2952	0.3244
23	(0.2878, 0.4105)	0.2452	0.2694
24	(0.3058, 0.4381)	0.2176	0.2391
25	(0.2470, 0.4801)	0.1754	0.1927
26	(0.2474, 0.4868)	0.1686	0.1853
27	(0.2958, 0.4673)	0.1883	0.2070
28	(0.2599, 0.4890)	0.1665	0.1830
29	(0.3381, 0.4439)	0.2118	0.2327
30	(0.4991, 0.2644)	0.3913	0.4300
31	(0.3554, 0.4420)	0.2137	0.2348
32	(0.4823, 0.3107)	0.3449	0.3790
33	(0.4491, 0.3687)	0.2870	0.3153
34	(0.4115, 0.4168)	0.2389	0.2625
35	(0.4327, 0.4299)	0.2258	0.2481
36	(0.4169, 0.4459)	0.2098	0.2305
37	(0.3925, 0.4912)	0.1645	0.1808
38	(0.4071, 0.4807)	0.1749	0.1923
39	(0.5555, 0.3136)	0.3421	0.3759
40	(0.3335, 0.5454)	0.1101	0.1210
41	(0.5198, 0.3779)	0.2778	0.3053
42	(0.3383, 0.5556)	0.0999	0.1098
43	(0.4196, 0.4971)	0.1586	0.1743
44	(0.4844, 0.4524)	0.2033	0.2234

45	(0.5296, 0.4120)	0.2437	0.2678
46	(0.5970, 0.3208)	0.3349	0.3680
47	(0.4340, 0.5289)	0.1267	0.1392
48	(0.6233, 0.2929)	0.3428	0.3767
49	(0.3381, 0.6004)	0.0547	0.0601
50	(0.3436, 0.5936)	0.0311	0.0342

Appendix E. Proof of Proposition 1

Proof. Let

$$R(t) = y = 1 - \frac{1}{2}\left[1 + \frac{2}{\sqrt{\pi}}\int_0^{\frac{t-\mu}{\sigma\sqrt{2}}} e^{-l^2} dl\right] = 1 - \frac{1}{2}\left[1 + erf\left(\frac{t-\mu}{\sigma\sqrt{2}}\right)\right] = 1 - \frac{1}{2}[1 + erf(z)] \tag{50}$$

Take the Taylor's series expansion on error function $erf(z)$ and rearrange the equation, we have

$$1 - 2y = \frac{2}{\sqrt{\pi}}\sum_{n=0}^{\infty}\frac{z}{2n+1}\prod_{k=1}^{n}\frac{-z^2}{k} \tag{51}$$

Take the first two terms from the Taylor's series expansion, we have

$$1 - 2y = \frac{2}{\sqrt{\pi}}\left(z - \frac{z^3}{3}\right) \Longrightarrow z^3 - 3z + 3\sqrt{\pi}\left(\frac{1}{2} - y\right) = 0 \tag{52}$$

Let $p = -3,\ q = 3\sqrt{\pi}\left(\frac{1}{2} - y\right)$

$$z^3 - 3z + 3\sqrt{\pi}\left(\frac{1}{2} - y\right) = z^3 + pz + q = 0 \tag{53}$$

We have therefore deduced the Taylor's series expansion of Eq. (51) in the format of a depressed cubic. By Cardano's formula, if p and q are real numbers and $4p^2 + 27q^2 > 0$, the depressed cubic has real root solution. In Eq. (53), it is obvious that $4p^2 + 27q^2 = 36 + 243\pi\left(\frac{1}{2} - y\right)^2 > 0$, the real root z of Eq. (52), which is the inverse function of the normal distribution format of the reliability model is:

$$F_{Normal}{}^{-1}(x) = \mu + \sigma\sqrt{\pi}\left(\sqrt[3]{-\frac{3}{2}\sqrt{\pi}(\frac{1}{2} - x) + \sqrt{\frac{9}{4}\pi(\frac{1}{2} - x)^2 - 1}} + \sqrt[3]{-\frac{3}{2}\sqrt{\pi}(\frac{1}{2} - x) - \sqrt{\frac{9}{4}\pi(\frac{1}{2} - x)^2 - 1}}\right) \quad \square \tag{54}$$

Appendix F. Proof of Proposition 2

Proof. It is obvious that:

$$f(t_c) = \frac{\partial(1 - R(t_c, t_h))}{\partial t_c} = -\frac{\partial R(t_c, T_h)}{\partial t_c} \tag{55}$$

and

$$f(t_h) = \frac{\partial(1 - R(t_c, t_h))}{\partial t_h} = -\frac{\partial R(T_c, t_h)}{\partial t_h} \tag{56}$$

This leads to the availability life on one time scale expressed as:

$$\begin{aligned}
L_{ac} &= R(T_c, T_h) \times T_c + [1 - R(T_c, T_h)]\frac{\int_0^{T_c} t_c f(t_c) dt_c}{1 - R(T_c, T_h)} \\
&= R(T_c, T_h) \times T_c + [1 - R(T_c, T_h)]\frac{\int_0^{T_c}\left(t_c - \frac{\partial R(t_c, T_h)}{\partial t_c}\right) dt_c}{1 - R(T_c, T_h)} \\
&= R(T_c, T_h) \times T_c + \int_0^{T_c} -t_c \partial R(t_c, T_h) \\
&= R(T_c, T_h) \times T_c + \left\{\left[-t_c R(t_c, T_h)\right]_0^{T_c} + \int_0^{T_c} R(t_c, T_h) dt_c\right\} \\
&= R(T_c, T_h) \times T_c - T_c R(T_c, T_h) + \int_0^{T_c} R(t_c, T_h) dt_c \\
&= \int_0^{T_c} R(t_c, T_h) dt_c
\end{aligned} \tag{57}$$

Similarly,

$$L_{ah} = \int_0^{T_h} R(T_c, t_h) dt_h \tag{58}$$

Therefore,

$$L_a = \sqrt{{L_{ac}}^2 + {L_{ah}}^2} = \sqrt{\left[\int_0^{T_c} R(t_c, T_h) dt_c\right]^2 + \left[\int_0^{T_h} R(T_c, t_h) dt_h\right]^2} \quad \square \tag{59}$$

Appendix G. Proof of Lemma 1, Corollaries 1.1 and 1.2 and Proposition 3

Proof of Lemma 1. Assume a fixed value of $T_h' \in [0,1]$. A plane at T_h', $\alpha T_h' + \delta = 0$, parallel to plane $t_c - O - R$ cuts the reliability surface $R(t_c, t_h)$. The projection of R on plane $\alpha T_h' + \delta = 0$ is $R_c(t_c, T_h')$. With $f_c = -\frac{\partial R_c}{\partial t_c}$. To simplify the expression we mark $R_c(t_c, T_h')$ as $R_c(t_c)$.

We have

$$
\begin{aligned}
\frac{\partial^2 W}{\partial {T_c}^2} &= -f_c(T_c)\left\{\int_0^{T_c} R_c(t_c)dt_c + R_c(T_c)\bar{M}_{pc} + \left[1 - R_c(T_c)\right]\bar{M}_{cc}\right\} + R_c(T_c)\left\{R_c(T_c) - f_c(T_c)\bar{M}_{pc} + f_c(T_c)\bar{M}_{cc}\right\} \\
&\quad - R_c(T_c)\left\{R_c(T_c) - f_c(T_c)\bar{M}_{pc} + f_c(T_c)\bar{M}_{cc}\right\} - \int_0^{T_c} R_c(t_c)dt_c\left\{-f_c(T_c) - \frac{\partial f_c(T_c)}{\partial T_c}\bar{M}_{pc} + \frac{\partial f_c(T_c)}{\partial T_c}\bar{M}_{cc}\right\} \\
&= -f_c(T_c)\left\{\int_0^{T_c} R_c(t_c)dt_c + R_c(T_c)\bar{M}_{pc} + \left[1 - R_c(T_c)\right]\bar{M}_{cc}\right\} - \int_0^{T_c} R_c(t_c)dt_c\left\{-f_c(T_c) - \frac{\partial f_c(T_c)}{\partial T_c}\bar{M}_{pc} + \frac{\partial f_c(T_c)}{\partial T_c}\bar{M}_{cc}\right\} \\
&= -f_c(T_c)\int_0^{T_c} R_c(t_c)dt_c - f_c(T_c)R_c(T_c)\bar{M}_{pc} - f_c(T_c)\left[1 - R_c(T_c)\right]\bar{M}_{cc} + \int_0^{T_c} R_c(t_c)dt_c f_c(T_c) + \int_0^{T_c} R_c(t_c)dt_c\frac{\partial f_c(T_c)}{\partial T_c}\bar{M}_{pc} \\
&\quad - \int_0^{T_c} R_c(t_c)dt_c\frac{\partial f_c(T_c)}{\partial T_c}\bar{M}_{cc} \\
&= -f_c(T_c)\bar{M}_{cc} + (\bar{M}_{pc} - \bar{M}_{cc})\left[\int_0^{T_c} R_c(t_c)dt_c\frac{\partial f_c(T_c)}{\partial T_c} - R_c(T_c)f_c(T_c)\right] \\
&= -f_c(T_c)\bar{M}_{cc} + (\bar{M}_{pc} - \bar{M}_{cc})\frac{\partial\int_0^{T_c} R_c(t_c)dt_c}{\partial f_c(T_c)} \\
&= -f_c(T_c)\bar{M}_{cc} + (\bar{M}_{pc} - \bar{M}_{cc})\frac{\partial\iint_0^{T_c} f_c(t_c)dt_c dt_c}{\partial f_c(T_c)} \\
&= -f_c(T_c)\bar{M}_{cc} - (\bar{M}_{cc} - \bar{M}_{pc})T_c\frac{\partial\int_0^{T_c} f_c(t_c)dt_c}{\partial f_c(T_c)} \\
&\leqq -f_c(T_c)\bar{M}_{cc} - (\bar{M}_{cc} - \bar{M}_{pc})T_c f_c(T_c) < 0
\end{aligned}
\tag{60}
$$

On the condition of

$$
\bar{M}_{cc} > \bar{M}_{pc} \Rightarrow \bar{M}_{cc} - \bar{M}_{pc} > 0 \quad \square \tag{61}
$$

Proof of Corollary 1.1. Symmetrically, assume a fixed value of $T_c' \in [0,1]$. A plane at T_c', $\beta T_c' + \delta = 0$, parallel to plane $t_h - O - R$ cuts the reliability surface $R(t_c, t_h)$. The projection of R on plane $\beta T_c' + \delta = 0$ is $R_h(T_c', t_h)$. With $f_h = -\frac{\partial R_h}{\partial t_h}$. To simplify the expression we mark $R_h(T_c', t_h)$ as $R_h(t_h)$. We have

$$
\begin{aligned}
\frac{\partial^2 W}{\partial {T_h}^2} &= -f_h(T_h)\left\{\int_0^{T_h} R_h(t_h)dt_h + R_h(T_h)\bar{M}_{ph} + \left[1 - R_h(T_h)\right]\bar{M}_{ch}\right\} + R_h(T_h)\left\{R_h(T_h) - f_h(T_h)\bar{M}_{ph} + f_h(T_h)\bar{M}_{ch}\right\} \\
&\quad - R_h(T_h)\left\{R_h(T_h) - f_h(T_h)\bar{M}_{ph} + f_h(T_h)\bar{M}_{ch}\right\} - \int_0^{T_h} R_h(t_h)dt_h\left\{-f_h(T_h) - \frac{\partial f_h(T_h)}{\partial T_h}\bar{M}_{ph} + \frac{\partial f_h(T_h)}{\partial T_h}\bar{M}_{ch}\right\} \\
&= -f_h(T_h)\left\{\int_0^{T_h} R_h(t_h)dt_h + R_h(T_h)\bar{M}_{ph} + \left[1 - R_h(T_h)\right]\bar{M}_{ch}\right\} - \int_0^{T_h} R_h(t_h)dt_h\left\{-f_h(T_h) - \frac{\partial f_h(T_h)}{\partial T_h}\bar{M}_{ph} + \frac{\partial f_h(T_h)}{\partial T_h}\bar{M}_{ch}\right\} \\
&\leqq -f_h(T_h)\bar{M}_{ch} - (\bar{M}_{ch} - \bar{M}_{ph})T_h f_h(T_h) < 0
\end{aligned}
\tag{62}
$$

On the condition of

$$
\bar{M}_{ch} > \bar{M}_{ph} \Rightarrow \bar{M}_{ch} - \bar{M}_{ph} > 0 \quad \square \tag{63}
$$

Proof of Corollary 1.2. Consider any local extrema point $T^{(k,k)}\left({T_c}^{(k)}, {T_h}^{(k)}\right), k \in [1,n]$ on the surface of $W(t_c, t_h)$, the gradient at point $T^{(k,k)}$ is $\nabla W = \frac{\partial W}{\partial {T_c}^{(k)}}\mathbf{i} + \frac{\partial W}{\partial {T_h}^{(k)}}\mathbf{j}$. Here, vector $\mathbf{i}$ is the unit vector on the t_c-axis, and vector $\mathbf{j}$ is the unit vector on the t_h-axis. Comparing to the previous local extrema point $T^{(k,k-1)}\left({T_c}^{(k)}, {T_h}^{(k-1)}\right)$, the component vector of the gradient on the t_h-axis at $T^{(k,k)}$ is $\frac{\partial W}{\partial {T_h}^{(k)}}\mathbf{j} = 0$. As $T^{(k,k)}$ is local extrema, it is obvious that $\left|\frac{\partial W}{\partial {T_h}^{(k-1)}}\mathbf{j}\right| > 0$, the increment in gradient on the t_h-axis is $\triangle(\nabla W)^{(k_j)} = \left|\frac{\partial W}{\partial {T_h}^{(k-1)}}\mathbf{j}\right|$. Similarly, we have, $\left|\frac{\partial W}{\partial {T_c}^{(k-1)}}\mathbf{i}\right| > 0$, with each iteration the increment in gradient on the t_c-axis, is $\triangle(\nabla W)^{(k_i)} = \left|\frac{\partial W}{\partial {T_c}^{(k-1)}}\mathbf{i}\right|$. Therefore, it is proved that the iteration algorithm moves the value towards the monotonically increased gradient direction of the value of W. While by Lemma 1 and Corollary 1.1, the availability function W is differentiable within the entire domain, which leads to the local extrema to increase until convergence, the limit of the convergence infinitely approaches global extrema. $\square$

Proof of Proposition 3. The Hessian of the availability function W is:

$$
H_W(T_c, T_h) = \begin{bmatrix} \frac{\partial^2 W}{\partial {T_c}^2} & \frac{\partial^2 W}{\partial T_c \partial T_h} \\ \frac{\partial^2 W}{\partial T_h \partial T_c} & \frac{\partial^2 W}{\partial {T_h}^2} \end{bmatrix} \tag{64}
$$

by Lemma 1 and Corollary 1.1 we have

$$\frac{\partial^2 W}{\partial {T_c}^2} < 0 \tag{65}$$

and

$$\frac{\partial^2 W}{\partial {T_h}^2} < 0 \tag{66}$$

By Corollary 1.2, we have:

$$\lim_{t_c \to T_c} \frac{\partial W}{\partial t_c} = 0 \tag{67}$$

and

$$\lim_{t_h \to T_h} \frac{\partial W}{\partial t_h} = 0 \tag{68}$$

Therefore, we have the determinant of the Hessian:

$$\left|H_W(T_c, T_h)\right| = \begin{vmatrix} \frac{\partial^2 W}{\partial {T_c}^2} & \frac{\partial^2 W}{\partial T_c \partial T_h} \\ \frac{\partial^2 W}{\partial T_h \partial T_c} & \frac{\partial^2 W}{\partial {T_h}^2} \end{vmatrix} \to \lim_{t_c \to T_c, t_h \to T_h} \begin{vmatrix} \frac{\partial^2 W}{\partial {T_c}^2} & \frac{\partial^2 W}{\partial T_c \partial T_h} \\ \frac{\partial^2 W}{\partial T_h \partial T_c} & \frac{\partial^2 W}{\partial {T_h}^2} \end{vmatrix} = \lim_{t_c \to T_c, t_h \to T_h} \left(\frac{\partial^2 W}{\partial {T_c}^2} \frac{\partial^2 W}{\partial {T_h}^2} - \frac{\partial^2 W}{\partial T_c \partial T_h} \frac{\partial^2 W}{\partial T_h \partial T_c} \right) > 0 \tag{69}$$

Prove that the availability function W has global extrema at (T_c, T_h) □

References

[1] Zhou H, Lopes Genez TA, Brintrup A, Parlikad AK. A hybrid-learning decomposition algorithm for competing risk identification within fleets of complex engineering systems. Reliab Eng Syst Saf 2022;217:107992. http://dx.doi.org/10.1016/j.ress.2021.107992, [Online]. Available: https://www.sciencedirect.com/science/article/pii/S0951832021005020.

[2] Yıldırım Ş, Yıldız B. Electric bus fleet composition and scheduling. Transp Res C 2021;129:103197. http://dx.doi.org/10.1016/j.trc.2021.103197, [Online]. Available: https://www.sciencedirect.com/science/article/pii/S0968090X21002126.

[3] de Pater I, Mitici M. Predictive maintenance for multi-component systems of repairables with remaining-useful-life prognostics and a limited stock of spare components. Reliab Eng Syst Saf 2021;214:107761. http://dx.doi.org/10.1016/j.ress.2021.107761, [Online]. Available: https://www.sciencedirect.com/science/article/pii/S095183202100288X.

[4] Cao Y, Ding Y, Jia M, Tian R. A novel temporal convolutional network with residual self-attention mechanism for remaining useful life prediction of rolling bearings. Reliab Eng Syst Saf 2021;107813. http://dx.doi.org/10.1016/j.ress.2021.107813, [Online]. Available: https://www.sciencedirect.com/science/article/pii/S0951832021003355.

[5] Ding Y, Jia M, Miao Q, Huang P. Remaining useful life estimation using deep metric transfer learning for kernel regression. Reliab Eng Syst Saf 2021;212:107583. http://dx.doi.org/10.1016/j.ress.2021.107583, [Online]. Available: https://www.sciencedirect.com/science/article/pii/S0951832021001332.

[6] Zang Y, Shangguan W, Cai B, Wang H, Pecht MG. Hybrid remaining useful life prediction method. a case study on railway D-cables. Reliab Eng Syst Saf 2021;213:107746. http://dx.doi.org/10.1016/j.ress.2021.107746, [Online]. Available: https://www.sciencedirect.com/science/article/pii/S0951832021002775.

[7] Liu J, Lei F, Pan C, Hu D, Zuo H. Prediction of remaining useful life of multi-stage aero-engine based on clustering and LSTM fusion. Reliab Eng Syst Saf 2021;214:107807. http://dx.doi.org/10.1016/j.ress.2021.107807, [Online]. Available: https://www.sciencedirect.com/science/article/pii/S0951832021003306.

[8] Wen P, Zhao S, Chen S, Li Y. A generalized remaining useful life prediction method for complex systems based on composite health indicator. Reliab Eng Syst Saf 2021;205:107241. http://dx.doi.org/10.1016/j.ress.2020.107241, [Online]. Available: https://www.sciencedirect.com/science/article/pii/S0951832020307419.

[9] Xiang S, Qin Y, Liu F, Gryllias K. Automatic multi-differential deep learning and its application to machine remaining useful life prediction. Reliab Eng Syst Saf 2022;223:108531. http://dx.doi.org/10.1016/j.ress.2022.108531, [Online]. Available: https://www.sciencedirect.com/science/article/pii/S0951832022001855.

[10] Xu F, Yang F, Fei Z, Huang Z, Tsui K-L. Life prediction of lithium-ion batteries based on stacked denoising autoencoders. Reliab Eng Syst Saf 2021;208:107396. http://dx.doi.org/10.1016/j.ress.2020.107396, [Online]. Available: https://www.sciencedirect.com/science/article/pii/S0951832020308838.

[11] Xu X, Tang S, Yu C, Xie J, Han X, Ouyang M. Remaining useful life prediction of lithium-ion batteries based on Wiener process under time-varying temperature condition. Reliab Eng Syst Saf 2021;214:107675. http://dx.doi.org/10.1016/j.ress.2021.107675, [Online]. Available: https://www.sciencedirect.com/science/article/pii/S0951832021002131.

[12] Infante V, Freitas M, Fonte M. Failure analysis of a crankshaft of a helicopter engine. Eng Fail Anal 2019;100:49–59. http://dx.doi.org/10.1016/j.engfailanal.2019.01.072, [Online]. Available: https://www.sciencedirect.com/science/article/pii/S1350630718314833.

[13] Zhang J, Dai H, Lin J, Yuan Y, Liu Z, Sun Y, Ding K. Cracking analysis of an aero-engine combustor. Eng Fail Anal 2020;115:104640. http://dx.doi.org/10.1016/j.engfailanal.2020.104640, [Online]. Available: https://www.sciencedirect.com/science/article/pii/S1350630718310331.

[14] Ejaz N, Qureshi I, Rizvi S. Creep failure of low pressure turbine blade of an aircraft engine. Eng Fail Anal 2011;18(6):1407–14. http://dx.doi.org/10.1016/j.engfailanal.2011.03.010, [Online]. Available: https://www.sciencedirect.com/science/article/pii/S135063071100063X.

[15] Zhang H, Li C, Guo Q, Ma Z, Li H, Liu Y. Improving creep resistance of nickel-based superalloy Inconel 718 by tailoring gamma double prime variants. Scr Mater 2019;164:66–70. http://dx.doi.org/10.1016/j.scriptamat.2019.01.041, [Online]. Available: https://www.sciencedirect.com/science/article/pii/S1359646219300582.

[16] Zhu S-P, Huang H-Z, He L-P, Liu Y, Wang Z. A generalized energy-based fatigue–creep damage parameter for life prediction of turbine disk alloys. Eng Fract Mech 2012;90:89–100. http://dx.doi.org/10.1016/j.engfracmech.2012.04.021, [Online]. Available: https://www.sciencedirect.com/science/article/pii/S0013794412001609.

[17] Song L-K, Bai G-C, Fei C-W. Dynamic surrogate modeling approach for probabilistic creep-fatigue life evaluation of turbine disks. Aerosp Sci Technol 2019;95:105439. http://dx.doi.org/10.1016/j.ast.2019.105439, [Online]. Available: https://www.sciencedirect.com/science/article/pii/S1270963819322229.

[18] Zhou H, Brintrup A, Parlikad AK. Module failure feature detection by cluster analysis for fleets of civil aircraft engines. IFAC-PapersOnLine 2021;54(1):31–6. http://dx.doi.org/10.1016/j.ifacol.2021.08.154, 17th IFAC Symposium on Information Control Problems in Manufacturing INCOM 2021, [Online]. Available: https://www.sciencedirect.com/science/article/pii/S2405896321009186.

[19] Su Z, Jamshidi A, Núñez A, Baldi S, De Schutter B. Multi-level condition-based maintenance planning for railway infrastructures – A scenario-based chance-constrained approach. Transp Res C 2017;84:92–123. http://dx.doi.org/10.1016/j.trc.2017.08.018, [Online]. Available: https://www.sciencedirect.com/science/article/pii/S0968090X17302292.

[20] Jamshidi A, Hajizadeh S, Su Z, Naeimi M, Núñez A, Dollevoet R, De Schutter B, Li Z. A decision support approach for condition-based maintenance of rails based on big data analysis. Transp Res C 2018;95:185–206. http://dx.doi.org/10.1016/j.trc.2018.07.007, [Online]. Available: https://www.sciencedirect.com/science/article/pii/S0968090X18309859.

[21] Su Z, Jamshidi A, Núñez A, Baldi S, De Schutter B. Integrated condition-based track maintenance planning and crew scheduling of railway networks. Transp Res C 2019;105:359–84. http://dx.doi.org/10.1016/j.trc.2019.05.045, [Online]. Available: https://www.sciencedirect.com/science/article/pii/S0968090X18304339.

[22] Chen L, Wang J, Yang W. A single machine scheduling problem with machine availability constraints and preventive maintenance. Int J Prod Res 2021;59(9):2708–21. http://dx.doi.org/10.1080/00207543.2020.1737336, eprint: [Online]. Available: https://doi.org/10.1080/00207543.2020.1737336.

[23] Liu B, Liang Z, Parlikad AK, Xie M, Kuo W. Condition-based maintenance for systems with aging and cumulative damage based on proportional hazards model. Reliab Eng Syst Saf 2017;168:200–9. http://dx.doi.org/10.1016/j.ress.2017.04.010, Maintenance Modelling, [Online]. Available: https://www.sciencedirect.com/science/article/pii/S0951832016308857.

[24] Erguido A, Crespo Márquez A, Castellano E, Gómez Fernández J. A dynamic opportunistic maintenance model to maximize energy-based availability while reducing the life cycle cost of wind farms. Renew Energy 2017;114:843–56. http://dx.doi.org/10.1016/j.renene.2017.07.017, [Online]. Available: https://www.sciencedirect.com/science/article/pii/S0960148117306304.
[25] Zhou H, Li F, Le Blanc M, Pan J. A Bayesian inference reliability evaluation on the corrosion-affected underground high-voltage power grid. Int J Reliab Qual Safety Eng 2022;29(01):2150042. http://dx.doi.org/10.1142/S021853932150042X, eprint: [Online]. Available:.
[26] Kaplan EL, Meier P. Nonparametric Estimation from Incomplete Observations. J Amer Statist Assoc 1958;53(282):457–81. http://dx.doi.org/10.2307/2281868, [Online]. Available: http://www.jstor.org/stable/2281868.
[27] Durante F, Fernández-Sánchez J, Sempi C. A topological proof of Sklar's theorem. Appl Math Lett 2013;26(9):945–8. http://dx.doi.org/10.1016/j.aml.2013.04.005, [Online]. Available: http://www.sciencedirect.com/science/article/pii/S0893965913001183.
[28] Kole E, Koedijk K, Verbeek M. Selecting copulas for risk management. J Bank Financ 2007;31(8):2405–23. http://dx.doi.org/10.1016/j.jbankfin.2006.09.010, [Online]. Available: http://www.sciencedirect.com/science/article/pii/S0378426607000362.
[29] Demarta S, McNeil AJ. The t copula and related copulas. Internat Statist Rev 2005;73(1):111–29. http://dx.doi.org/10.1111/j.1751-5823.2005.tb00254.x, eprint: arXiv:https://onlinelibrary.wiley.com/doi/pdf/10.1111/j.1751-5823.2005.tb00254.x.
[30] Fiix. Preventive maintenance. 2021, Accessed: 2021-06-08. [Online]. Available: https://www.fiixsoftware.com/maintenance-strategies/preventative-maintenance/.